Molecular Structures and Magnetic Resonance Spectroscopic Investigations of Highly Distorted Six-Coordinate Low-Spin Iron(III) Porphyrinate Complexes

Hiroshi Ogura,[†] Liliya Yatsunyk,[†] Craig J. Medforth,[‡] Kevin M. Smith,[‡] Kathleen M. Barkigia,[§] Mark W. Renner,[§] Dan Melamed,[§] and F. Ann Walker*,[†]

Contribution from the Department of Chemistry, University of Arizona, Tucson, Arizona 85721-0041, Department of Chemistry, University of California, Davis, California 95616, and Energy Sciences and Technology Department, Brookhaven National Laboratory, Upton, New York 11973-5000

Received November 22, 2000. Revised Manuscript Received May 3, 2001

Abstract: Three bis-axially ligated complexes of iron(III) octaethyltetraphenylporphyrin, (OETPP)Fe^{III}, have been prepared, which are low-spin complexes, each with two axial nitrogen-donor ligands (*N*-methylimidazole (*N*-MeIm), 4-(dimethylamino)pyridine (4-NMe_2Py), and 2-methylimidazole (2-MeImH)). The crystal and molecular structure of the bis-(2-MeImH) complex shows the macrocycle to be in a saddled conformation, with the ligands in perpendicular planes aligned at 14° to the porphyrin nitrogens so as to relieve the steric interaction between the 2-methyl groups and the porphyrin. The Fe−N(por) bond lengths are typical of nonplanar six-coordinate low-spin Fe^{III} complexes, while the axial Fe−N(ax) bond lengths are substantially longer than those of $[(TPP)Fe(2\text{-}MeImH)_2]^+$ (2.09(2) Å as compared to 2.015(4) and 2.010(4) Å). The crystal and molecular structure of the bis-(4-NMe_2Py) complex also shows the macrocycle to be in a mainly saddled conformation, but with a significant ruffled component. As a result, the average Fe−N(por) bonds are significantly shorter (1.951 Å as compared to 1.974 Å) than those of the bis-(2-MeImH) complex. One ligand is aligned at 9° to two trans porphyrin nitrogens, while the other is at 79° to the same porphyrin nitrogens, producing a dihedral angle of 70° between the ligand planes. The EPR spectrum of this complex, like that of the bis-(2-MeImH) complex, is of the "large g_{max}" type, with $g_{max} = 3.29$ and 3.26, respectively. However, in frozen CD_2Cl_2, $[(OETPP)Fe(N\text{-}MeIm)_2]^+$ exhibits both "large g_{max}" and normal rhombic signals, suggesting the presence of both "perpendicular" and "parallel" ligand orientations. The 1- and 2D ^{1}H NMR spectra of each of these complexes, as well as the chloroiron(III) starting material, were investigated as a function of temperature. The COSY and NOESY/EXSY spectra of the chloride complex are consistent with the expected *J*-coupling and saddle inversion dynamics, respectively. Complete spectral assignments for the bis-(*N*-MeIm) and -(4-NMe_2-Py) complexes have been made using 2D ^{1}H NMR techniques. In each case, the number of resonances due to methylene (two) and phenyl protons (one each) is consistent with D_{2d} symmetry, and therefore an effective perpendicular orientation of the axial ligands on the time scale of the NMR experiments. The temperature dependences of the ^{1}H resonances of these complexes show significant deviations from Curie behavior, and also evidence of extensive ligand exchange and rotation. Spectral assignment of the eight methylene resonances of the bis-(2-MeImH) complex to the four ethyl groups was possible through the use of 2D ^{1}H NMR techniques. The complex is fluxional, even at −90 °C, and ROESY data suggest that the predominant process is saddle inversion accompanied by simultaneous rotation of the axial ligands. Saddle inversion becomes slow on the 2D NMR time scale as the temperature is lowered in the ligand order of *N*-MeIm > 4-NMe_2Py > 2-MeImH, probably due mainly to progressive destabilization of the ground state rather than progressive stabilization of the transition state of the increasingly "hindered" bis-ligand complexes.

Introduction

Porphyrins and metalloporphyrins are conformationally flexible, and multiple macrocycle conformations have been observed crystallographically. In biological systems, distortions from planarity have been observed in photosynthetic reaction centers,[1,2] light-harvesting complexes,[1,2] heme proteins,[2−8] and methyl coenzyme M reductase.[2,9,10] Protein matrix interactions with the porphyrin may be responsible for the macrocycle

* To whom correspondence should be addressed. FAX: 520-626-9300. E-mail: awalker@u.arizona.edu.
† University of Arizona.
‡ University of California, Davis.
§ Brookhaven National Laboratory.

(1) Huber, R. *Eur. J. Biochem.* **1990**, *187*, 283−305.
(2) Shelnutt, J. A.; Song, X.-Z.; Ma, J.-G.; Jai, S.-L.; Jentzen, W.; Medforth, C. J. *Chem. Soc. Rev.* **1998**, *27*, 31−41 and references therein.
(3) Hobbs, J. D.; Shelnutt, J. A. *J. Protein Chem.* **1995**, *14*, 19−25.
(4) Martinez, S. E.; Smith, J. L.; Huang, D.; Szczepaniak, A.; Cramer, W. A. In *Research in Photosynthesis*; Murata, N., Ed.; Proceedings of the IXth International Congress on Photosynthesis, Vol. 2; Kluwer Academic: Dordrecht, The Netherlands, 1992; p 495.
(5) Alden, R. G.; Ondrias, M. R.; Shelnutt, J. A. *J. Am. Chem. Soc.* **1990**, *112*, 691−697.
(6) Schlichting, I.; Berendzen, J.; Philips, G. N., Jr; Sweet, R. M. *Nature* **1994**, *371*, 808−812.
(7) Jentzen, W.; Ma, J.-G.; Shelnutt, J. A. *Biophys. J.* **1998**, *74*, 753−763.
(8) Ma, J.-G.; Zhang, J.; Franco, R.; Jia, S.-L.; Moura, I.; Moura, J. J. G.; Kroneck, P. M. H.; Shelnutt, J. A. *Biochemistry* **1998**, *37*, 12431−12442.

10.1021/ja004053s CCC: $20.00
Published on Web 06/13/2001

distortions from planarity in vivo that could modulate their physical and chemical properties. In model compounds, nonplanar distortions of the macrocycle can be induced by steric interactions between the peripheral substituents[11−19] or between porphyrin and axial ligands,[20−29] by protonation and N-substitution,[30] by bridging the macrocycle with short-chain alkyl groups,[31,32] by insertion of a metal or nonmetal whose radius does not match the size of the porphyrin hole,[9,33−35] or by partial saturation of the macrocycle.[9,11,36] Distortions may also be induced by electronic factors such as bonding interactions with π-acid ligands that stabilize the d_π orbitals of the metal, which, for low-spin Fe(III), produce the $(d_{xz},d_{yz})^4(d_{xy})^1$ ground state in which the d_{xy}−porphyrin π-interaction can occur only if the porphyrin ring ruffles.[25,37,38]

Nonplanar distortions of the macrocycle have been shown to alter the mixing of the atomic orbitals and the relative energy and symmetry of the molecular orbitals,[11] which in turn can modify the electronic structure,[11,20,25,37−44] reduction potentials,[11,30,45−48] and magnetic[17,20,38,49] and vibrational properties[11,50,51] of various nonplanar porphyrins. Macrocycle distortion also causes the formation of cavities that can orient planar axial ligands. Recent crystallographic[21,22,24−26,52−58] and NMR spectroscopic studies[17−19,23,27−29,37,59−64] of highly substituted metalloporphyrins indicate that the macrocycle adopts a predominantly S_4 (saddled or ruffled)[52] geometry, although waving and doming contributions are also frequently observed.[2,65] The ruffling and saddling distortions result in each case in the formation of mutually perpendicular cavities above and below the macrocycle plane;[23,51] these cavities are capable of orienting planar axial ligands over the *meso* carbons for ruffled distortions, or above the pyrrole nitrogens for saddled distortions. This has been confirmed by crystallographic[21,22,24−26,53−58] and magnetic resonance studies[16,18−20,22−29,38,59−64] of nonplanar metalloporphyrins with planar axial ligands, and has also been investigated by molecular mechanics calculations.[16,51,60] As found in these

(9) Eschenmoser, A. *Ann. N. Y. Acad. Sci.* **1986**, *471*, 108−129.
(10) Thauer, R. K. *Microbiology* **1998**, *144*, 2377−2406.
(11) Barkigia, K. M.; Chantranupong, L.; Smith, K. M.; Fajer, J. *J. Am. Chem. Soc.* **1988**, *110*, 7566−7567.
(12) Barkigia, K. M.; Berber, M. D.; Fajer, J.; Medforth, C. J.; Renner, M. W.; Smith, K. M. *J. Am. Chem. Soc.* **1990**, *112*, 8851−8857.
(13) Medforth, C. J.; Senge, M. O.; Smith, K. M.; Sparks, L. D.; Shelnutt, J. A. *J. Am. Chem.* Soc. **1992**, *114*, 9859−9869.
(14) Marsh, R. E.; Schaeffer, W. P.; Hodge, J. A.; Hughes, M. E.; Gray, H. B.; Lyons, J. E.; Ellis, P. E., Jr. *Acta Crystallogr.* **1993**, *C49*, 1339−1342.
(15) Jentzen, W.; Simpson, M. C.; Hobbs, J. D.; Song, X.; Ema, T.; Nelson, N. Y.; Medforth, C. J.; Smith, K. M.; Veyrat, M.; Mazzanti, M.; Ramasseul, R.; Marchon, J. C.; Takeuchi, T.; Goddard, W. A., III; Shelnutt, J. A. *J. Am. Chem. Soc.* **1995**, *117*, 11085−11097.
(16) Medforth, C. J.; Muzzi, C. M.; Smith, K. M.; Abraham, R. J.; Hobbs, J. D.; Shelnutt, J. A. *J. Chem. Soc., Chem. Commun.* **1994**, 1843−1844.
(17) Cheng, R. J.; Chen, P. Y.; Gau, P. R.; Chen, C. C.; Peng, S. M. *J. Am. Chem. Soc.* **1997**, *119*, 2563−2569.
(18) Medforth, C. J.; Muzzi, C. M.; Shea, K. M.; Smith, K. M.; Abraham, R. J.; Jia, S.; Shelnutt, J. A. *J. Chem. Soc., Perkin Trans. 2* **1997**, 833−837.
(19) Nakamura, M.; Yamaguchi, T.; Ohgo, Y. *Inorg. Chem.* **1999**, *38*, 3126−3131.
(20) Walker, F. A.; Huynh, B. H.; Scheidt, W. R.; Osvath, S. R. *J. Am. Chem. Soc.* **1986**, *108*, 5288−5297.
(21) Scheidt, W. R.; Kirner, J. L.; Hoard, J. L.; Reed, C. A. *J. Am. Chem. Soc.* **1987**, *109*, 1963−1968.
(22) Safo, M. K.; Gupta, G. P.; Walker, F. A.; Scheidt, W. R. *J. Am. Chem. Soc.* **1991**, *113*, 5497−5510.
(23) Walker, F. A.; Simonis, U. *J. Am. Chem. Soc.* **1991**, *113*, 8652−8657; **1992**, *114*, 1929.
(24) Safo, M. K.; Gupta, G. P.; Watson, C. T.; Simonis, U.; Walker, F. A.; Scheidt, W. R. *J. Am. Chem. Soc.* **1992**, *114*, 7066−7075.
(25) Safo, M. K.; Walker, F. A.; Raitsimring, A. M.; Walters, W. P.; Dolata, D. P.; Debrunner, P. G.; Scheidt, W. R. *J. Am. Chem. Soc.* **1994**, *116*, 7760−7770.
(26) Munro, O. Q.; Marques, H. M.; Debrunner, P. G.; Mohanrao, K.; Scheidt, W. R. *J. Am. Chem. Soc.* **1995**, *117*, 935−954.
(27) Nakamura, M.; Ikezaki, A. *Chem. Lett. (Jpn.)* **1995**, 733−734.
(28) Nakamura, M.; Kawasaki, Y. *Chem. Lett. (Jpn.)* **1996**, 805−806.
(29) Polam, J. R.; Shokhireva, T. Kh.; Raffii, K.; Simonis, U.; Walker, F. A. *Inorg. Chim. Acta* **1997**, *263*, 109−117.
(30) Senge, M. O. In *The Porphyrin Handbook*; Kadish, K. M., Smith, K. M., Guilard, R., Eds.; Academic Press: San Diego, CA; 2000, Chapter 6, Vol. 1, pp 239−347.
(31) Simonis, U.; Walker, F. A.; Lee, P. L.; Hanquet, B. J.; Meyerhoff, D. J.; Scheidt, W. R. *J. Am. Chem. Soc.* **1987**, *109*, 2659−2668.
(32) Maiti, N. C.; Ravikanth, M. *J. Chem. Soc., Faraday Trans.* **1996**, *92*, 1095−1100.
(33) Ryu, S.; Whang, D.; Kim, J.; Yeo, W.; Kim, K. *J. Chem. Soc., Dalton Trans.* **1993**, 205−209.
(34) Medforth, C. J.; Senge, M. O.; Forsyth, T. P.; Hobbs, J. D.; Shelnutt, J. A.; Smith, K. M. *Inorg. Chem.* **1994**, *33*, 3865−3872.
(35) Yamamoto, Y.; Nadano, R.; Itagaki, M.; Akiba, K.-y. *J. Am. Chem. Soc.* **1995**, *117*, 8287−8288.
(36) Scheer, H. In *The Porphyrins, Vol. 2, Structure and Synthesis, Part B*; Dolphin, D., Ed.; Academic Press: New York, 1978; pp 1−90.
(37) Walker, F. A.; Nasri, H.; Turowska-Tyrk, I.; Mohanrao, K.; Watson, C. T.; Shokhirev, N. V.; Debrunner, P. G.; Scheidt, W. R. *J. Am. Chem. Soc.* **1996**, *118*, 12109−12118.
(38) Walker, F. A. *Coord. Chem. Rev.* **1999**, *185−186*, 471−534.
(39) Dolphin, D. *J. Heterocycl. Chem.* **1970**, *7*, 275−283.
(40) Medforth, C. J.; Berber, M. D.; Smith, K. M.; Shelnutt, J. A. *Tetrahedron Lett.* **1990**, *31*, 3719−3722.
(41) Ema, T.; Senge, M. O.; Nelson, N. Y.; Ogoshi, H.; Smith, K. M. *Angew. Chem., Int. Ed. Engl.* **1994**, *33*, 1879−1881.
(42) Gentemann, S.; Medforth, C. J.; Forsyth, T. P.; Nurco, D. J.; Smith, K. M.; Fajer, J.; Holten, D. *J. Am. Chem. Soc.* **1994**, *116*, 7363−7368.
(43) Takeuchi, T.; Gray, H. B.; Goddard, W. A., III. *J. Am. Chem. Soc.* **1994**, *116*, 9730−9732.
(44) Birnbaum, E. R.; Schaefer, W. P.; Labinger, J. A.; Bercaw, J. E.; Gray, H. B. *Inorg. Chem.* **1995**, *34*, 1751−1755.
(45) Kadish, K. M.; Van Caemelbecke, E.; Boulas, P.; D'Souza, F.; Vogel, E.; Kisters, M.; Medforth, C. J.; Smith, K. M. *Inorg. Chem.* **1993**, *32*, 4177−4178.
(46) Ochsenbein, P.; Ayougou, K.; Mandon, D.; Fischer, J.; Weiss, R.; Austin, R. N.; Jayaraj, K.; Gold, A.; Terner, J.; Fajer, J. *Angew. Chem., Int. Ed. Engl.* **1994**, *33*, 348−350.
(47) Chen, H. L.; Ellis, P. E., Jr.; Wijesekera, T.; Hagan, T. E.; Groh, S. E.; Lyons, J. E.; Ridge, D. P. *J. Am. Chem. Soc.* **1994**, *116*, 1086−1089.
(48) Hodge, J. A.; Hill, M. G.; Gray, H. B. *Inorg. Chem.* **1995**, *34*, 809−812.
(49) Schünemann, V.; Gerdan, M.; Trautwein, A. X.; Haoudi, N.; Mandon, D.; Fischer, J.; Weiss, R.; Tabard, A.; Guilard, R. *Angew. Chem., Int. Ed. Engl.* **1999**, *38*, 3181−3183.
(50) Shelnutt, J. A.; Majumder, S. A.; Sparks, L. D.; Hobbs, J. D.; Medforth, C. J.; Senge, M. O.; Smith, K. M.; Miura, M.; Luo, L.; Quirke, J. M. E. *J. Raman Spectrosc.* **1992**, *23*, 523−529.
(51) Sparks, L. D.; Medforth, C. J.; Park, M. S.; Chamberlain, J. R.; Ondrias, M. R.; Senge, M. O.; Smith, K. M.; Shelnutt, J. A. *J. Am. Chem. Soc.* **1993**, *115*, 581−592.
(52) Scheidt, W. R.; Lee, Y. J. *Struct. Bonding* **1987**, *64*, 1−70.
(53) Bang, H.; Edwards, J. O.; Kim, J.; Lawler, R. G.; Reynolds, K.; Ryan, W. J.; Sweigart, D. A. *J. Am. Chem. Soc.* **1992**, *114*, 2843−2852.
(54) Barkigia, K. M.; Renner, M. W.; Furenlid, L. R.; Medforth, C. J.; Smith, K. M.; Fajer, J. *J. Am. Chem. Soc.* **1993**, *115*, 3627−3635.
(55) Regev, A.; Galili, T.; Medforth, C. J.; Smith, K. M.; Barkigia, K. M.; Fajer, J.; Levanon, H. *J. Phys. Chem.* **1994**, *98*, 2520−2526.
(56) Grinstaff, M. W.; Hill, M. G.; Birnbaum, E. R.; Schaefer, W. P.; Labinger, J. A.; Gray, H. B. *Inorg. Chem.* **1995**, *34*, 4896−4902.
(57) Renner, M. W.; Barkigia, K. M.; Melamed, D.; Smith, K. M.; Fajer, J. *Inorg. Chem.* **1996**, *35*, 5120−5121.
(58) Renner, M. W.; Barkigia, K. M.; Fajer, J. *Inorg. Chim. Acta* **1997**, *263*, 181−187.
(59) Wolowiec, S.; Latos-Grazynski, L.; Mazzanti, M.; Marchon, J. C. *Inorg. Chem.* **1997**, *36*, 5761−5771.
(60) Medforth, C. J.; Hobbs, J. D.; Rodriguez, M. R.; Abraham, R. J.; Smith, K. M.; Shelnutt, J. A. *Inorg. Chem.* **1995**, *34*, 1333−1341.
(61) Shokhirev, N. V.; Shokhireva, T. Kh.; Polam, J. R.; Watson, C. T.; Raffii, K.; Simonis, U.; Walker, F. A. *J. Phys. Chem. A* **1997**, *101*, 2778−2886.
(62) Momot, K. I.; Walker, F. A. *J. Phys. Chem. A* **1997**, *101*, 2787−2795.
(63) Momot, K. I.; Walker, F. A. *J. Phys. Chem. A* **1997**, *101*, 9207−9216.
(64) Momot, K. I.; Walker, F. A. *J. Phys. Chem. A* **1998**, *102*, 10682−10688.
(65) Nurco, D. J.; Medforth, C. J.; Forsyth, T. P.; Olmstead, M. M.; Smith, K. M. *J. Am. Chem.* Soc. **1996**, *118*, 10918−10919.

model hemes, it is expected that for heme proteins, the axial ligands and their relative orientation can alter the electronic and magnetic properties,[20,38] as well as the reduction potentials.[20,30]

For ferriheme complexes with $(d_{xy})^2(d_{xz},d_{yz})^3$ electronic ground states (the most common electron configuration for low-spin ferrihemes in biological systems), rhombic EPR spectra have been associated with mutually parallel orientation of the axial ligand planes, and "large g_{max}" EPR spectra with mutually perpendicular ligand planes.[20,21] However, how perfectly perpendicular the axial ligands must be to give rise to a "large g_{max}" EPR spectrum, or how nearly degenerate the d_{xz} and d_{yz} orbitals of the heme must be,[20] has remained a question. On the basis of their "large g_{max}" EPR spectra,[20,22,24−26,66,67] the membrane-bound bis-histidine-coordinated *b* cytochromes[68−81] are believed to have their imidazole rings in perpendicular planes. However, when model heme complexes with perpendicular ligand planes are reduced to low-spin iron(II), the axial ligands are found to be in parallel planes and the macrocycles are not ruffled, but rather are strictly planar.[82] Although one crystal structure has been reported of a strongly saddled perhalogenated iron(II) porphyrinate bound to two pyridine ligands in perpendicular planes,[56] for macrocycles such as tetramesitylporphyrin that have the possibility of being *either* planar or ruffled, it was only possible to stabilize a ruffled macrocycle with axial ligands in perpendicular planes for low-spin Fe(II) at extremely low temperatures (−70 to −90 °C) using sterically bulky axial ligands (1,2-Me_2Im).[29] Thus, if given the choice, low-spin Fe(II) porphyrinates appear to prefer axial ligands in parallel planes. At the present time, the resolutions of the structures of the cytochrome bc_1 complexes reported thus far[70,71] are just beginning to reach the point where the axial ligand orientations can be estimated.[83] Therefore, the preparation and investigation of model heme complexes that can test hypotheses regarding the relationship between easily obtainable spectroscopic data and actual predictions of axial ligand plane orientations is still very much needed.

The membrane-bound bis-histidine-coordinated cytochromes of mitochondrial complexes II and III and the similar cytochromes of chloroplasts do not lose their axial ligands upon redox.[68−81] In the oxidized state, we know from the "large g_{max}" EPR spectra that the imidazole planes of the histidine ligands have "near-perpendicular" dihedral angles, yet we also know that low-spin Fe(II) porphyrinates prefer not to have perpendicular ligand planes with a ruffled ring conformation.[29,82] This, plus the expected rigidity of the axial ligand orientation in a membrane-bound protein, makes it unlikely that the membrane-bound cytochromes that exhibit "large g_{max}" EPR signals have their axial ligands lying over the *meso* positions in perpendicular planes. On the other hand, it has also become clear that perfect alignment of axial ligands in either strictly parallel or perpendicular planes is not required to produce normal rhombic vs "large g_{max}" EPR signals, respectively. This is because a study of two bis-(5-methylimidazole) complexes of (TMP)Fe^{III} has shown that a normal rhombic EPR spectrum is observed when the axial ligand plane dihedral angle is as large as 30°, while a "large g_{max}" EPR spectrum is observed when the dihedral angle is as small as 78°.[84] In an attempt to determine how much closer to each other these dihedral angles might be pushed without interconverting the EPR spectral type, as well as to determine whether alignment of the axial ligands near the N(por)−Fe−N(por) axes in near-perpendicular planes would provide a means for stabilizing the same ligand orientations for both low-spin Fe(III) and low-spin Fe(II), the present investigations of bis-ligand complexes of (OETPP)Fe(III) were initiated.

In this work, we present X-ray crystallographic structural data, polycrystalline and frozen solution EPR, and variable-temperature 1- and 2D NMR spectroscopic studies of iron(III) complexes of octaethyltetraphenylporphyrin (OETPP), a highly substituted porphyrin that maintains a saddle shape in both the solid state and solution. A series of metal complexes of OETPP have been shown by X-ray crystallography to have steric interactions between the peripheral substituents that cause the porphyrin to distort in a saddled conformation.[12,19,52,54] This porphyrin is used for two purposes: First, OETPP is used for modeling the structural and dynamic properties of nonplanar biological hemes. X-ray crystallographic and detailed dynamic NMR studies were carried out for this purpose. Second, OETPP is used for modeling the EPR properties of bis-histidine-ligated biological ferrihemes,[67−81] by using the cavities to orient the axial ligands in near-perpendicular planes, but not over the *meso* positions, where ruffling is encouraged.

Experimental Section

Synthesis. Octaethyltetraphenylporphyrin ($OETPPH_2$) and its iron(III) complex were synthesized by the previously reported methods.[12,51] Iron insertion for the sample utilized for NMR spectroscopy was carried out by slight modification of the method described previously.[51] The porphyrin (17 mg) was reacted with 80 mg of $FeCl_2 \cdot 4H_2O$ in 25 mL of refluxing DMF in the presence of air and absence of light. The reaction was monitored spectrophotometrically and was complete within 30 min. The resulting iron(III) porphyrinate was chromatographed on a column of neutral alumina, using 10:1 $CHCl_3/CH_3OH$ as eluant. The solvent was removed, and the solid was dissolved in 25 mL of CH_2Cl_2 and treated with 100 mL of 1 M NaCl/0.2 M HCl in order to replace any adventitious anions such as hydroxide with chloride.[85] The organic phase was dried repeatedly over NaCl, and the solvent was removed using a rotary evaporator. The yield of the metalloporphyrin was nearly quantitative.

X-ray Crystallography. (a) $[(OETPP)Fe(2\text{-}MeImH)_2]^+$. $FeN_4C_{60}H_{60} \cdot 2(C_4N_2H_6) \cdot 0.33(SbF_6) \cdot 0.667(Cl)$ crystallized from 2-chlorobutane/

(66) Walker, F. A.; Reis, D.; Balke, V. L. *J. Am. Chem. Soc.* **1984**, *106*, 6888−6898.
(67) Salerno, J. C. *J. Biol. Chem.* **1984**, *259*, 2331−2336.
(68) Widger, W. R.; Cramer, W. A.; Herrmann, R. G.; Trebst, A. *Proc. Natl. Acad. Sci. U.S.A.* **1984**, *81*, 674−678.
(69) Salerno, J. C.; Xu, Y.; Osgood, M. P.; Kim, C. H.; King, T. E. *J. Biol. Chem.* **1989**, *264*, 15398−15403 and references therein.
(70) Xia, D.; Yu, C.-A.; Kim, H.; Xia, J.-Z.; Kachurin, A. M.; Zhang, L.; Yu, L.; Deisenhofer, J. *Science* **1997**, *277*, 60−66.
(71) Iwata, S.; Lee, J. W.; Okada, K.; Lee, J. K.; Iwata, M.; Rasmussen, B.; Link, T. A.; Ramaswamy, S.; Jap, S. K. *Science* **1998**, *281*, 64−71.
(72) Yang, X.; Trumpower, B. L. *J. Biol. Chem.* **1988**, *263*, 11962−11970.
(73) Hobbs, J. D.; Kriauciunas, A.; Güner, S.; Knaff, D. B.; Ondrias, M. R. *Biochim. Biophys. Acta* **1990**, *1018*, 47−54.
(74) Salerno, J. C.; McGill, J. W.; Gerstle, G. C. *FEBS Lett.* **1983**, *162*, 257−261.
(75) Furbacher, P. N.; Girvin, M. E.; Cramer, W. A. *Biochemistry* **1989**, *28*, 8990−8998.
(76) Babcock, G. T.; Widger, W. R.; Cramer, W. A.; Oertling, W. A.; Metz, J. *Biochemistry* **1985**, *24*, 3638−3645.
(77) Berry, E. A.; Guergova-Kuras, M.; Huang, L.-S.; Crofts, A. R. *Annu. Rev. Biochem.* **2000**, *69*, 1005−1075.
(78) Fridén, H.; Cheesman, M. R.; Hederstedt, L.; Andersson, K. K.; Thomson, A. J. *Biochim. Biophys. Acta* **1990**, *1041*, 207−215.
(79) Hägerhäll, C.; Aasa, R.; von Wachenfeldt, C.; Hederstedt, L. *Biochemistry* **1992**, *31*, 7411−7421.
(80) Hägerhäll, C.; Hederstedt, L. *FEBS Lett.* **1996**, *389*, 25−31.
(81) Hägerhäll, C. *Biochim. Biophys. Acta* **1997**, *1320*, 107−141.
(82) Safo, M. K.; Nesset, M. J. M.; Walker, F. A.; Debrunner, P. G.; Scheidt, W. R. *J. Am. Chem. Soc.* **1997**, *119*, 9438−9448.
(83) Iwata, S. Personal communication.
(84) Munro, O. Q.; Serth-Guzzo, J. A.; Turowska-Tyrk, I.; Mohanrao, K.; Shokhireva, T. K.; Walker, F. A.; Debrunner, P. G.; Scheidt, W. R. *J. Am. Chem. Soc.* **1999**, *121*, 11144−11155.
(85) Basu, P.; Raitsimring, A. M.; LaBarre, M. J.; Dhawan, I. K.; Weibrecht, J. L.; Enemark, J. H. *J. Am. Chem. Soc.* **1994**, *116*, 7166−7176.

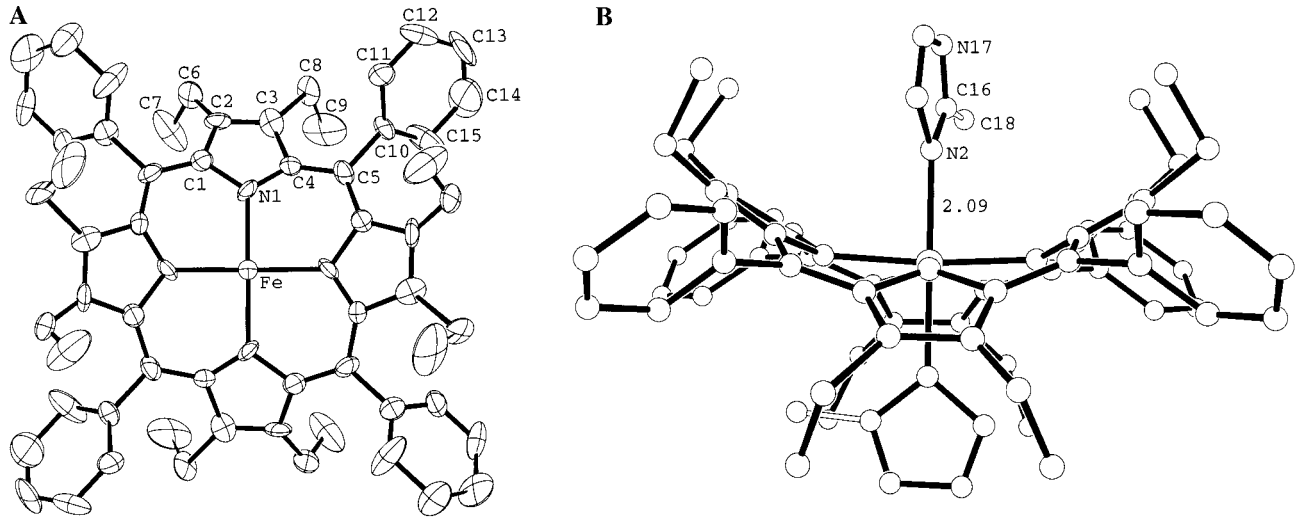

Figure 1. (A) Molecular structure and atom names for the macrocycle of $[(OETPP)Fe(2\text{-}MeImH)_2]^+$. The thermal ellipsoids enclose 50% probability, and hydrogens are omitted for clarity. (B) Edge-on view of $[(OETPP)Fe(2\text{-}MeImH)_2]^+$ and atom names for the axial ligands.

2-propanol in space group $F\bar{4}3c$ with the following cell parameters: $a = b = c = 34.363(2)$ Å, $\alpha = \beta = \gamma = 90°$, $V = 40576.4(41)$ Å^3, $Z = 24$. Data were collected at Brookhaven National Laboratory at 200 K on an Enraf-Nonius CAD4 diffractometer with Cu Kα radiation in the range $5.14 \le 2\theta \le 129.4°$. A total of 1753 reflections ($0 \le h \le k \le l < \infty$) were measured, with 1527 remaining after the *hkl* extinctions were removed. Refinement with SHELXL93[86] yielded $R1 = 0.093$, w$R2 = 0.176$ for $I > 2\sigma(I)$ and $R1 = 0.257$ and w$R2 = 0.358$ for 1523 reflections. The high value of w$R2$ stems from disorder of the axial 2-methylimidazoles and partial occupancies of the counterions, which leave only 816 of 1527 reflections observed. Due to incomplete metathesis of the Cl^- precursor with SbF_6^-, the counterions are a mixture of SbF_6^- and Cl^-.

(b) $[(OETPP)Fe(4\text{-}NMe_2Py)_2]^+$. $FeN_4C_{60}H_{60}\cdot 2(C_7N_2H_{10})\cdot(Cl)\cdot 4(CDCl_3)$ crystallized from chloroform-*d*/cyclohexane in space group $Pna2_1$ with the following cell parameters: $a = 34.849(3)$ Å, $b = 13.6506(13)$ Å, $c = 17.1170(16)$ Å, $\alpha = \beta = \gamma = 90°$, $V = 8142.6(13)$ Å^3, $Z = 4$. Data were collected at the University of Arizona at 170 K on a CCD-equipped Bruker SMART1000 diffractometer with Mo Kα radiation in the range $3.20 \le 2\theta \le 49.48°$. A total of 77 014 reflections (13 836 unique) were integrated and retained. Of the unique reflections, 7583 were found to fulfill the condition $I > 2\sigma(I)$. Refinement with SHELX v. 5.0[86] yielded $R1 = 0.0582$ and w$R2 = 0.1341$ for 7583 reflections. The final anisotropic full-matrix least-squares refinement based on F^2 of all reflections converged at $R1 = 0.1380$, w$R2 = 0.1683$, and GoF = 0.960.

EPR Spectroscopy. EPR spectra were recorded on a Bruker ESP-300E spectrometer (operating at 9.4 GHz with 100 kHz field modulation) equipped with an Oxford Instruments ESR 900 continuous-flow liquid helium cryostat. The EPR spectra of the bis-(2-MeImH) and bis-(4-NMe_2Py) complexes were obtained both as polycrystalline solids and as frozen solutions in CD_2Cl_2, while the spectra of [(OETPP)-FeCl] and the bis-(*N*-MeIm) complex were obtained only in frozen CD_2Cl_2 solution. The microwave power was 2 mW for the bis-(2-MeImH) complex, 0.5 mW for the bis-(4-NMe_2Py) complex, and 0.2 mW for the bis-(*N*-MeIm) complex, each with a modulation amplitude of 3−4 G.

NMR Spectroscopy. The NMR samples of the bis-(*N*-MeIm) and bis-(4-NMe_2Py) complexes were prepared by adding 3−4 equiv of the ligand to 3 mg of (OETPP)FeCl in 0.3 mL of CD_2Cl_2 in an NMR sample tube. For preparation of the 2-MeImH complex, 3 mg of the chloride complex was dissolved in 0.3 mL of CD_2Cl_2, and a batch of preweighed 2-MeImH (6 equiv relative to 1 equiv of the porphyrin complex) was transferred quantitatively into the NMR tube. All NMR samples were degassed with argon.

The ^{1}H NMR data were collected at the University of Arizona on a Varian Unity-300 spectrometer operating at 299.956 MHz and equipped with an inverse probe. The temperature was calibrated using a methanol sample (Wilmad WGH-09) and the standard Varian calibration curve.[87] T_1 relaxation times were measured by first obtaining spectra using the inversion−recovery pulse sequence, and then fitting the data to an exponential. For the magnitude-mode COSY-45, DQF-COSY, and phase-sensitive NOESY/EXSY experiments, the standard pulse sequences were used.[88] A standard pulse sequence was used also for the phase-sensitive ROESY experiments.[89]

The Felix 95 and 2000 software packages (Molecular Simulations) were used for processing the 2D data. For the COSY data, squared sine bell function apodization or Lorentz−Gaussian transformation was applied before each of the two Fourier transformations. For the NOESY and ROESY data, linear prediction was applied to twice the original data size of both dimensions, and then Gaussian function apodization (parameters included in the figure captions) was applied. Baseline correction was applied to each segment of both dimensions, by determining the baseline points by FLATT[90] and then fitting these points to a fourth-order polynomial.

Results and Discussion

Structure of the Bis-(2-methylimidazole) Complex, $[(OETPP)Fe(2\text{-}MeImH)_2]^+$. Experimental crystallographic details for this complex are provided in Table S1 of the Supporting Information. Because the Fe atom in $[(OETPP)Fe(2\text{-}MeImH)_2]^+$ sits on a $\bar{4}$ position, only one-fourth of the porphyrin is unique: this is reflected in the nomenclature of the atoms (Figure 1). Also, due to the symmetry found for the crystal, the ligands are two-fold disordered; i.e., half of the methyl group site C18 is occupied by a hydrogen, and half of N17 is occupied by a carbon, and the asymmetric unit thus consists of only one-half of a 2-methylimidazole moiety. The $\bar{4}$- and 2-fold axes are coincident.

The saddle shape of the macrocycle of $[(OETPP)Fe(2\text{-}MeImH)_2]^+$ is evident in Figures 1 and 2, as well as in the linear display shown in Figure S1 of the Supporting Information. The C_β positions of each pyrrole ring are alternately displaced by ±1.23 and ±1.20 Å from the 24-atom mean plane, and the *meso*

(86) Sheldrick, G. M. *SHELXTL, Version 5.0*; Siemens Analytical X-ray Instruments, Inc.: Madison, WI, 1995.

(87) Variable Temperature Systems: Installation and Maintenance. (Pub. No. 87-195402-00, Rev. D0393); Varian Associates: Palo Alto, CA, 1993; p 43.

(88) Neuhaus, D.; Williamson, M. *The Nuclear Overhauser Effect in Structural and Conformational Analysis*; VCH: New York, 1989; p 263.

(89) Bax, A.; Davis, D. G. *J. Magn. Reson.* **1985**, *63*, 207−213.

(90) Güntert, P.; Wüthrich, K. *J. Magn. Reson.* **1992**, *96*, 403−407.

Table 1. Comparisons of Structural Parameters for (OETPP)Fe^{III} and Related Complexes

compound (counterion)	M−N(por), Å	av dihedral angle of phenyls (deg)	av $\|\Delta C_\beta\|$, 0.01 Å[a]	av $\|\Delta C_m\|$, 0.01 Å[a]	Fe−N(ax), Å	angle between N−Fe−N axis and ligand planes (deg)	dihedral angle between axial ligands (deg)
$[(OETPP)Fe(2\text{-}MeImH)_2]^+$ $(0.33SbF_6^-, 0.67Cl^-)$[b]	1.974(9)	42	120, 123	9	2.09(2)	14, 14	90
$[(OETPP)Fe(4\text{-}NMe_2Py)_2]^+$ (Cl^-)[b]	1.951(5)	66	111(3), 134(5)	28(2)	1.984(5) 2.015(6)	9, 29	70
$[(TPP)Fe(2\text{-}MeImH)_2]^+$ (ClO_4^-)[21]	1.971(4)	76	17(16)	40(1)	2.015(4) 2.010(4)	32, 32	89
$[(TMP)Fe(1,2\text{-}Me_2Im)_2]^+$ (ClO_4^-)[26]	1.937(12)	87	23, 24	68	2.004(5) 2.004(5)	45, 45	90
$[(TMP)Fe(4\text{-}NMe_2Py)_2]^+$ (ClO_4^-)[20]	1.964(10)	79	20(13)	51(5)	1.989(4) 1.978(4)	37, 42	79
$[(TMP)Fe(N\text{-}MeIm)_2]^+$	1.988(20)	81	2(2)	1(1)	1.975(3)	23	0
(ClO_4^-)[20]	1.987(1)	81	7(2)	8(1)	1.965(3)	41	0
(OETPP)FeCl[17]	2.031(5)	45	108, 123	19			
(OETPP)FeCl[49]	2.027(6) 2.053(5)	46	103, 124	22			
(OETPP)Co(II)[51]	1.929(3)	46	117	5.3			
(OETPP)Ni(II)[54]	1.906(2)	43	123	5			
(OETPP)Cu(II)[51]	1.977(5)	47	113	4.1			
(OETPP)Zn(MeOH)[12]	2.063(5)	46	108	5.0			
$OETPPH_2$[55]		43	117	4			

[a] Deviation from the mean plane of the 24-atom porphyrinate ring. [b] This work.

carbons lie ±0.09 Å out of plane, causing a slight ruffle, which is, however, much smaller than that observed in the high-spin complex, [(OETPP)FeCl],[17,49] or the bis-(4-NMe_2Py) complex discussed below (Table 1). In comparison to $[(OETPP)Fe(2\text{-}MeImH)_2]^+$, the porphyrin skeleton of $[(TPP)Fe(2\text{-}MeImH)_2]^+$ is more ruffled but less distorted overall.[21] As a consequence of the steep saddle distortion, the dihedral angles of the phenyl rings at the C_m positions shrink to 42° from 62, 78, 75, and 90° in $[(TPP)Fe(2\text{-}MeImH)_2]^+$.[21] This does not necessarily mean that there is increased interaction between the phenyl rings and the C_α of the porphyrin, however. The phenyl dihedral angles of purely saddled porphyrins are all smaller than those of purely ruffled porphyrins, as suggested by the data of Table 1. However, although phenyl−porphyrin *plane* angles decrease significantly for the saddling distortion, the dihedral angle between the phenyl and the C_α−N−C_α planes (which control the $\pi-\pi$ interactions) do not decrease nearly as much.

The bond distances and displacements from the mean plane of the atoms of the macrocycle (Figure 2) fall within the spread of literature values observed for low-spin iron(III) porphyrinates (Table 1). For example, the Fe−N1 distance of 1.974(9) Å is shorter than the canonical value of 1.990 Å for hexacoordinated planar low-spin iron(III) porphyrinates,[91] but is typical of nonplanar six-coordinate low-spin iron(III) porphyrinates.[21,22,24−26] The elongation of the axial Fe−N2 bond (2.09(2) Å, compared with 2.015(4) and 2.010(4) Å in $[(TPP)Fe(2\text{-}MeImH)_2]^+$ [21]) provides a means for alleviating steric contacts between the methyl groups and the porphyrin. In $[(TPP)Fe(2\text{-}MeImH)_2]^+$,[21] the axial ligand methyl group and the porphyrin are separated from each other by an alternative mechanism, namely tipping of the Fe−N bonds from the mean plane normal by 4°. In both structures, the closest contacts of the methyl groups to the atoms of the porphyrin are similar, 3.07 and 3.08 Å in $[(TPP)Fe(2\text{-}MeImH)_2]^+$ [21] vs 3.12 Å for $[(OETPP)Fe(2\text{-}MeImH)_2]^+$ (this work).

In the case of $[(TPP)Fe(2\text{-}MeImH)_2]^+$ [21] and $[(TMP)Fe(1,2\text{-}Me_2Im)_2]^+$,[26] the average Fe−N(por) distances are 1.971(4) and 1.937(12) Å, respectively, and they both have ruffled macrocycle cores. Even though the macrocycle core is more distorted in $[(OETPP)Fe(2\text{-}MeImH)_2]^+$ than in $[(TMP)Fe(1,2\text{-}Me_2Im)_2]^+$,[26] the Fe−N(por) distances are much shorter in the latter (1.974(9) vs 1.937(12) Å, respectively, Table 1). This again suggests that Fe−N(por) distances are sensitive to the distortion mode, i.e., saddled versus ruffled; as pointed out previously, ruffling tends to contract the porphyrin core more than other distortion modes (saddling, doming, waving).[92] Atomic coordinates, complete bond lengths and angles, anisotropic thermal parameters, and hydrogen coordinates are listed in Tables S2−S5, respectively, in the Supporting Information.

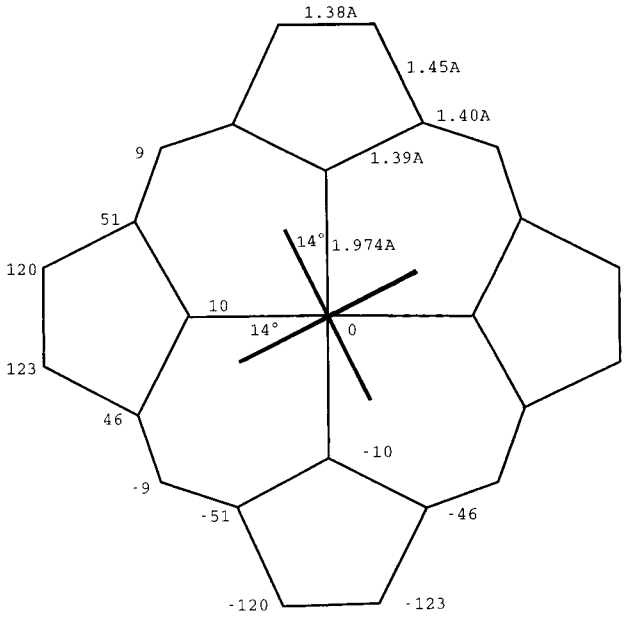

Figure 2. Average bond distances in $[(OETPP)Fe(2\text{-}MeImH)_2]^+$, displacements Δ from the average of the 24-atom porphyrin core in units of 0.01 Å, and axial ligand plane orientations.

The saddle distortion and the average positioning of the ethyls give rise to two mutually perpendicular pockets that control the

(91) Collins, D. M.; Countryman, R.; Hoard, J. L. *J. Am. Chem. Soc.* **1972**, *94*, 2066−2072.

(92) Song, X.-Z.; Jaquinod, L.; Jentzen, W.; Nurco, D. J.; Jin, S.-L.; Khoury, R. G.; Ma, J.-G.; Medforth, C. J.; Smith, K. M.; Shelnutt, J. A. *Inorg. Chem.* **1998**, *37*, 2009−2019.

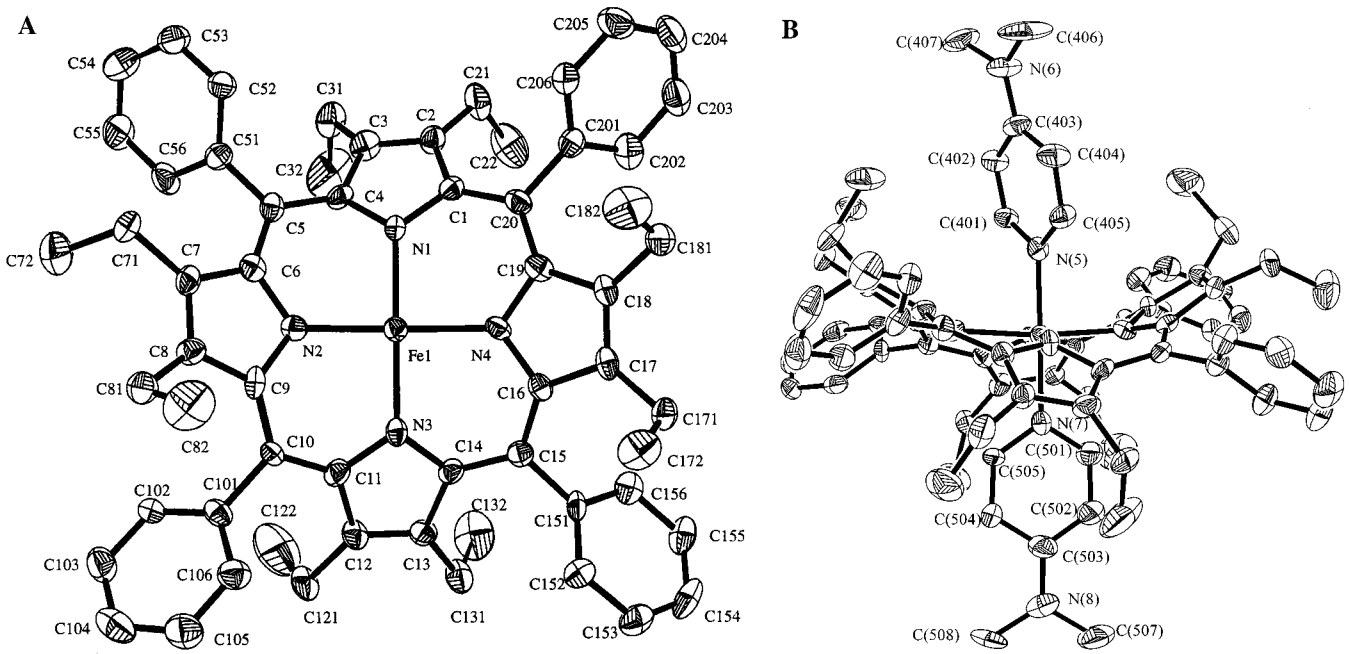

Figure 3. (A) Molecular structure and atom names for the macrocycle of $[(OETPP)Fe(4\text{-}NMe_2Py)_2]^+$. (B) Edge-on view of the complex and atom names for the axial ligands. The thermal ellipsoids enclose 50% probability, and hydrogens are omitted for clarity.

orientation of the axial ligands. Thus, the 2-methylimidazoles are oriented at 90° to each other. The orientation, however, is determined not only by the pockets, but also by the steric interaction between the ligands and the pyrrole N atoms, as is illustrated by the 14° rotation of the ligand planes to the ferriheme N−Fe−N axes (Table 1). For comparison, the ligands are poised at 89 and 82° for the two molecules in the unit cell of $[(OETPP)Fe(ImH)_2]^+$,[93] at 78° in $[(OETPP)Fe(Py)_2]^+$,[93] and at 70° in $[(OETPP)Fe(4\text{-}NMe_2Py)_2]^+$ (vide infra); also, in the ruffled $[(TPP)Fe(2\text{-}MeImH)_2]^+$,[21] the ligands are oriented at 32° to the N−Fe−N axes and are also perpendicular (89.3°) to each other. This shape-selective feature is also seen in other (OETPP)M complexes, including axially ligated Co^{II},[93] Ni^{II},[57] and Cu^{II} [58] complexes.

Structure of the Bis-(4-(dimethylamino)pyridine) Complex, $[(OETPP)Fe(4\text{-}NMe_2Py)_2]^+$. Experimental crystallographic details for this complex are provided in Table S6 in the Supporting Information. As shown in Figures 3 and 4, the porphyrin macrocycle of $[(OETPP)Fe(4\text{-}NMe_2Py)_2]^+$ adopts an overall saddled conformation with the average displacement of the β-pyrrole C atoms from the mean plane being 1.23 Å. However, more ruffling is present than in the case of the bis-(2-MeImH) complex, as indicated by the pronounced displacement of the *meso*-C atoms (±0.28 Å), the large dihedral angle of the *meso*-phenyl rings (60°), and the short Fe−N(por) distances (1.951(5) Å), which are more similar to those reported previously for the highly ruffled $[(TMP)Fe(4\text{-}NMe_2Py)_2]^+$ complex.[24] (Comparisons are summarized in Table 1.) While seven of the eight ethyl groups adopt the commonly observed axial conformation, the remaining ethyl (C71−C72) adopts the equatorial conformation. This suggests that the energy difference between axial and equatorial ethyl orientations is small,[60] and may in part be controlled by crystal packing interactions.

One of the axial ligands (N7, N8) is oriented at 9° to the N2−N4 axis. This offset from the orientation parallel to the macrocycle pocket appears to be caused by the steric repulsion between two porphyrin N atoms (N2, N4) and the pyridine 2,6-H

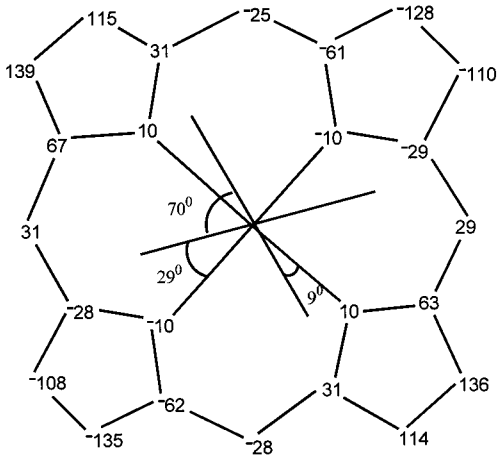

Figure 4. Displacements Δ from the average of the 24-atom porphyrin core of $[(OETPP)Fe(4\text{-}NMe_2Py)_2]^+$, in units of 0.01 Å, and axial ligand plane orientations.

atoms, and is smaller than that for the 2-MeImH ligands of the structure just discussed. The plane of the other axial ligand (N5, N6) forms a 29° angle with the N1−N3 axis. The resulting dihedral angle between the two axial ligands is 70°. The deviation of this angle from 90° may be caused by the Jahn−Teller effect[94] within the $(d_{xy})^2(d_{xz},d_{yz})^3$ ground-state system, which produces a static difference in energy of the d_{xz} and d_{yz} orbitals when the dihedral angle between axial ligand planes is less than 90°.[20,95] The fact that the deviation occurs despite the presence of the mutually perpendicular pockets confirms the observation of Medforth et al.,[18] that the potential energy curve for ligand rotation is fairly flat for a range of pyridine dihedral angles somewhat larger than the minimum-energy angle of ±10−14° from the N(por)−Fe−N(por) axes. For example, the potential energy for pyridine ligand orientations of 22.5° from

(93) Barkigia, K. M.; Melamed, D.; Renner, M. W.; Smith, K. M.; Fajer, J. Unpublished results.

(94) (a) Jahn, H. A.; Teller, E. *Proc. R. Soc.* **1937**, *A161*, 220. (b) Ballhausen, C. J. *Introduction to Ligand Field Theory*; McGraw-Hill: New York, 1962; p 193.

(95) Shokhirev, N. V.; Walker, F. A. *J. Biol. Inorg. Chem.* **1998**, *3*, 581−594, especially Figure 7.

that axis is only 2.1 kJ/mol higher than the minimum, but at larger angles the potential energy rises more steeply, reaching a maximum at 90° (123−133 kJ/mol).[18] The potential energy of the complexed six-membered ring pyridine at any angle is higher than that of the imidazole complex at the same angle, since the five-membered imidazole ring has a much smaller minimum-energy dihedral angle (2−3°) and rises more gently to a maximum at 90° (72−79 kJ/mol).[18] Furthermore, the driving force for small dihedral angles for axial ligands in a low-spin Fe(III) porphyrinate due to the unsymmetrical d_π electron configuration has been shown to be of similar magnitude to that for minimizing the potential energy by placing axial ligands in bulky porphyrinates in perpendicular planes.[84]

The degree of ruffling ($\Delta C_m = 0.28$) found for the [(OETPP)-Fe(4-NMe_2Py)$_2$]$^+$ complex is significantly greater than that for the bis-(2-MeImH) complex, and also much greater than those for the four-coordinate Co(II), Ni(II), and Cu(II) and five-coordinate Zn(II) complexes (0.053, 0.05, 0.041, and 0.050 Å, respectively).[12,51,54] Thus, while the OETPP ring system can be essentially purely saddled, strongly ruffled ring conformations that retain almost the same amount of saddle distortion as the purely saddled conformation are also possible, and thus provide a potential mechanism for macrocycle inversion. The large observed ligand plane angle of 29° for one of the 4-NMe_2Py ligands in this complex likewise suggests a close approach to the intermediate or transition state in the process of concurrent ligand rotation.

The two iron−axial ligand nitrogen bond distances of the bis-(4-NMe_2Py) complex are substantially different from each other: 2.015 Å for Fe−N7, and 1.984 Å for Fe−N5. The longer distance for the former reflects the steric interaction of the ligand with the porphyrin nitrogen atoms, while the shorter distance of the latter is made possible by the 29° rotation of the axial ligand from the N(por)−Fe−N(por) axis. Atomic coordinates, complete bond lengths and angles, anisotropic thermal parameters, and hydrogen coordinates are listed in Tables S7−S10 in the Supporting Information.

EPR Studies of [(OETPP)Fe(*N*-MeIm)$_2$]$^+$, [(OETPP)Fe-(4-NMe_2Py)]$^+$, and [(OETPP)Fe(2-MeImH)$_2$]$^+$. The X-band EPR spectrum of [(OETPP)Fe(*N*-MeIm)$_2$]Cl (CD_2Cl_2, 4.1 K, Figure 5, top panel) shows both rhombic ($g = 2.72, 2.38, 1.66$) and "large g_{max}" signals ($g = 3.12$). The "large g_{max}" signal is indicative of low-spin d^5 heme centers having axial ligands in "perpendicular" orientation[20,38] and is the expected type of EPR signal, based on the large dihedral angle expected due to the perpendicular "pockets". On the other hand, the rhombic signal is indicative of low-spin d^5 heme centers having axial ligand planes in "parallel" orientation, which, in its zero-degree dihedral angle limit, is difficult to rationalize with the presence of perpendicular ligand-binding pockets in (OETPP)Fe^{III}. For the bis-(*N*-MeIm) complex, the small tetragonal splitting Δ/λ[96] (2.79, compared to the values of 3−3.2 usually observed for bis-(imidazole) complexes of hemins[38]) may be a result of longer Fe−N_{ax} ligand bonds in [(OETPP)Fe(*N*-MeIm)$_2$]$^+$ compared to those of other bis-(*N*-MeIm) iron porphyrinate complexes.[93] The rhombic splitting, V/λ, is 2.58, yielding a value of the rhombicity, V/Δ, of 0.92, somewhat larger than the limiting value of 0.67 for the ideal case.[96] However, other larger values of the rhombicity have been reported recently.[38,97−99]

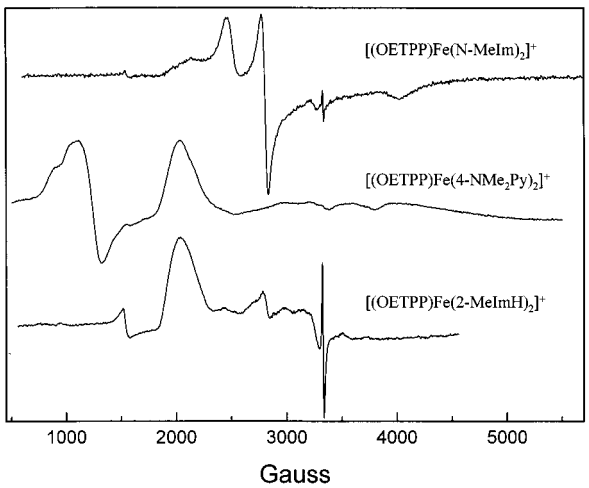

Figure 5. EPR spectra of [(OETPP)Fe(*N*-MeIm)$_2$]$^+$ (top) in frozen CD_2Cl_2 ($g = 3.12$ for the "large g_{max}" signal and $g = 2.72$, 2.38, and 1.66 for the normal rhombic signal), [(OETPP)Fe(4-NMe_2Py)$_2$]$^+$ (middle) in the solid state ($g = 3.29$ for the major peak near 2000 G), and [(OETPP)Fe(2-MeImH)$_2$]$^+$ (bottom) in methylene chloride at 4.2 K ($g = 3.26$ for the major peak near 2000 G). For [(OETPP)Fe(4-NMe_2Py)$_2$]$^+$ (middle), a large high-spin Fe(III) signal is also observed at $g = 6$ and 2, while for both frozen solution spectra, free radical impurity signals are seen at $g = 2$. All spectra were recorded at 4.2 K.

The EPR spectra of polycrystalline [(OETPP)Fe(4-NMe_2-Py)$_2$]$^+$ and of a frozen solution of [(OETPP)Fe(2-NMeImH)$_2$]Cl in CH_2Cl_2 (4.1 K, Figure 5, middle and bottom spectra, respectively) show "large g_{max}" signals. For the bis-(4-NMe_2Py) complex, this "large g_{max}" signal is also seen not only in the solid state ($g = 3.29$, Figure 5, middle) but also in frozen solution (CD_2Cl_2, $g = 3.28$, not shown), and was reported recently in CH_2Cl_2 for the perchlorate salt, $g = 3.24$,[100] but accompanied in all three media by no rhombic signal. The difference in the "large g_{max}" g-values of the bis-(4-NMe_2Py) and bis-(2-MeImH) complexes is less than experimental error (a magnetic field difference of 19 G for signals that are relatively broad), while the difference between these two g_{max} values and that of the bis-(*N*-MeIm) complex is greater than experimental error (a magnetic field difference of 90 G). The reason for the slightly smaller g_{max} value for the bis-(*N*-MeIm) complex is not known. For both the frozen solution spectrum of the bis-(2-MeImH) complex shown in Figure 5, and also that of the polycrystalline sample, several minor impurity signals (as well as a free radical signal) are also present near $g = 2$. Such signals are usually observed for "large g_{max}" type spectra,[20,66−68] and although they appear large in the derivative mode spectra, they represent only very small integrated signal areas relative to those of the "large g_{max}" species, and thus there is only a small percentage of sample with this type of EPR signal. Furthermore, "large g_{max}" species usually appear to be fairly weak in derivative mode because of short relaxation times compared to those of rhombic low-spin Fe(III) species. This fact also makes it difficult to quantify the relative amounts of "large g_{max}" and normal rhombic species present for the bis-(*N*-MeIm) complex, but it is estimated that the concentrations of the two species are at least similar (within a factor of 1.5−2.0).

A large high-spin Fe(III) signal is also present for the bis-(4-NMe_2Py) complex, probably due to loss of one ligand from molecules on the surface of the crystallites. This high-spin signal

(96) Taylor, C. P. S. *Biochim. Biophys. Acta* **1977**, *491*, 137−148.
(97) Raitsimring, A. M.; Borbat, P.; Shokhireva, T. Kh.; Walker, F. A. *J. Phys. Chem.* **1996**, *100*, 5235−5244.
(98) Schünemann, V.; Raitsimring, A. M.; Benda, R.; Trautwein, A. X.; Shokhireva, T. Kh.; Walker, F. A. *J. Biol. Inorg. Chem.* **1999**, *4*, 708−716.
(99) Astashkin, A. V.; Raitsimring, A. M.; Walker, F. A. *J. Am. Chem. Soc.* **2001**, *123*, 1905−1913.
(100) Ikue, T.; Yamaguchi, T.; Ohgo, Y.; Nakamura, M. *Chem. Lett. (Jpn.)* **2000**, 342−343.

disappeared when the crystallites were dissolved in CD_2Cl_2 and a small amount of excess 4-NMe_2Py was added to the sample before freezing (not shown).

As indicated above, the EPR spectrum of [(OETPP)Fe(*N*-MeIm)$_2$]Cl indicates the presence of two species, one with the axial ligands in nonperpendicular ("parallel") planes and the other with "perpendicular" orientations.[20,22,24−26,84] The rhombic signal cannot arise from perfectly parallel orientation of the axial ligands, considering the steric constraint of mutually perpendicular pockets in the porphyrin. On the other hand, although these pockets appear to favor the perpendicular orientation that gives rise to a "large g_{max}" spectrum, the crystal structure of the bis-(4-NMe_2Py) complex and molecular mechanics calculations on the bis-(imidazole) complex[18] indicate that the ligand orientations may deviate significantly from 90° dihedral angles with little increase in potential energy. One of the most important questions that arises from this work is the following: What is the dihedral angle of axial ligands that marks the transition between the two types of EPR spectra? A recent study of two crystalline forms of the bis-(5-methylimidazole) complex of (TMP)Fe^{III} indicates that the transition angle must be between 30 and 78°,[84] while the structure of [(OETPP)Fe(4-$NMe_2Py)_2$]$^+$ (vide supra) reduces the high angle limit to 70°. However, for the bis-(*N*-MeIm) complex in homogeneous solution, the axial ligands may have the choice of rotating in the same direction or in opposite directions because of the reduced steric hindrance of the *N*-MeIm ligand, thus producing two different dihedral angles, 90° and a much smaller dihedral angle. Based upon the 14° offset of the 2-MeImH ligands from the N(por)−Fe−N(por) axes, rotation of two less-hindered *N*-MeIm ligands in opposite directions could give a dihedral angle of 62° or less.

As mentioned above, molecular mechanics calculations on a number of bis-(pyridine) and -(imidazole) complexes of (OETPP)Co^{III} further suggest that the barrier to rotation of the axial ligands by up to 22.5° is fairly flat,[18] which could easily allow a dihedral angle of 45° for the two *N*-methylimidazole ligands, if they rotated in opposite directions. Whether the dihedral angle is as small as 45° or as large as 60°, and whether dihedral angles as large as the latter are still able to produce a normal rhombic EPR signal, are questions that will be addressed in future research. In any case, it is clear that the Jahn−Teller effect[94] exerts an important influence on the structure of these highly distorted low-spin iron(III) porphyrinates, in that it causes the complex to distort to the extent necessary to create a resultant ligand plane orientation that lifts the degeneracy of the d_{xz} and d_{yz} orbitals to the extent that the EPR spectral type can switch from "large g_{max}" to normal rhombic for some of the molecules in the frozen solution of [(OETPP)Fe(*N*-MeIm$_2$)]$^+$.

The membrane-bound bis-histidine-coordinated *b* cytochromes of mitochondrial complex III (also known as cytochrome bc_1 or ubiquinone-cytochrome *c* oxidoreductase) have heme centers b_H and b_L with very different reduction potentials (105,−70 or 70,−110 mV, respectively, vs NHE, depending on preparation,[69] for the bovine heart protein), yet both give rise to "large g_{max}" EPR signals (g_{max} = 3.44 and 3.78, respectively[67,69]). The structure of this protein complex has now been refined to 2.5 Å,[83] which allows the first estimates to be made of the orientations of the axial imidazole planes of the two histidine ligands of each heme. At this stage of refinement, for heme b_L, these angles appear to 36 and −47° to the N_{II}−N_{IV} (N_C−N_A crystallographic) axis, yielding a dihedral angle of ligand planes of 83° (with ligands lying near the *meso* positions, although Fe(II) complexes do not favor this configuration[29,82]). Because of the large angles to the porphyrin nitrogens, it may be expected that when refined to higher resolution, heme b_L will have a ruffled conformation similar to that of [(TMP)Fe(4-$NMe_2Py)_2$]$^+$,[22] although undoubtedly not nearly as ruffled. In contrast, for heme b_H, these angles appear to be 29 and −9° to the same axis of this heme, a dihedral angle of only 38°. Because of the small angles to the porphyrin nitrogens, it may be expected that when refined to higher resolution, heme b_H will have a conformation similar to that of the OETPP structures of this work, although probably not nearly as saddled because of the nonhindered imidazole (histidine) ligands. The dihedral angle of 38° for the axial imidazole planes seems small for a "large g_{max}" heme, and this is indeed the dihedral angle of the His-59 and histamine imidazole planes observed for nitrophorin 1-histamine,[101] which has a normal rhombic EPR signal.[101,102] Additional model heme complexes with axial ligand dihedral angles of greater than 30° but less than 70° are being prepared in order to determine whether the 38° angle is close to that where the EPR spectral type switches from normal rhombic to "large g_{max}" or, if not, what that angle is. It is hoped that the present and continuing work in our laboratories will be helpful to protein crystallographers in modeling the heme centers of large protein complexes.

Proton NMR and EPR Studies of the Chloride Complex, [(OETPP)FeCl]. The 1D ^{1}H NMR spectrum at 22 °C (Figure 6, top; listing of resonance assignments in Table 2) contains two methyl and four downfield-shifted methylene peaks and is consistent with both the C_{2v} symmetry of the molecule and the apparent stability of the axial conformation of the ethyl groups (i.e., pointing above the parts of the macrocycle that are saddled upward and below the parts that are saddled downward for a significantly greater fraction of the time than is spent on all other possible angular orientations).[60] The chemical shifts of the methylene protons found in the present study are essentially identical to those reported previously,[17,103] and the differences between the chemical shifts of this study and those reported by Cheng et al.[17] are due to differences in the solvation properties of the solvents used ($C_2D_2Cl_4$[17] and CD_2Cl_2[104]).

The methylene resonances for [(OETPP)FeCl] have a large spread, 21.3 ppm (CD_2Cl_2, 22 °C) compared to 3.6 ppm for [(OEP)FeCl][105] ($CDCl_3$, 29 °C). This spread is caused by either or both of the following: (1) The conformational freedom of the methylene group is low and therefore the McConnell *Q* values are more disparate for each individual proton; (2) the low symmetry (C_{2v}) removes the degeneracy between d_{xz} and d_{yz} and also between what would have been the two degenerate LUMOs in C_{4v}.[106−109] This causes asymmetry in the metal-to-porphyrin back-bonding and thus the spin density at the pyrrole

(101) Weichsel, A.; Andersen, J. F.; Champagne, D. E.; Walker, F. A.; Montfort, W. R. *Nature Struct. Biol.* **1998**, *5*, 304−309.

(102) Astashkin, A. V.; Raitsimring, A. M.; Walker, F. A. *Chem. Phys. Lett.* **1999**, *306*, 9−17.

(103) The low-temperature (200 K) spectra of this complex reported previously, with chemical shifts of 61.8, 57.0, 29.6, and 22.5 ppm,[49] agree with those of this study at somewhat lower temperature (181 K), if the most shifted methylene proton signal (79 ppm), which is quite broad, is ignored, with the fourth peak reported (at 22.5 ppm) being due to one of the ortho-phenyl resonances.

(104) Yatsunyk, L.; Shokhirev, N. V.; Walker, F. A. Manuscript in preparation.

(105) Walker, F. A.; La Mar, G. N. *Ann. N. Y. Acad. Sci.* **1973**, *206*, 328−348.

(106) La Mar, G. N.; Walker, F. A. In *The Porphyrins*; Dolphin, D., Ed.; Academic Press: New York, 1979; Vol. IV, pp 61−157.

(107) Walker, F. A.; Simonis, U. In *Biological Magnetic Resonance*; Berliner, L. J., Reuben, J., Eds.; Plenum Press: New York, 1993; Vol. 12, pp 133−274.

(108) Walker, F. A. In *The Porphyrin Handbook*; Kadish, K. M., Smith, K. M., Guilard, R., Eds.; Academic Press: San Diego, CA, 2000; Vol. 5, Chapter 36, pp 81−183.

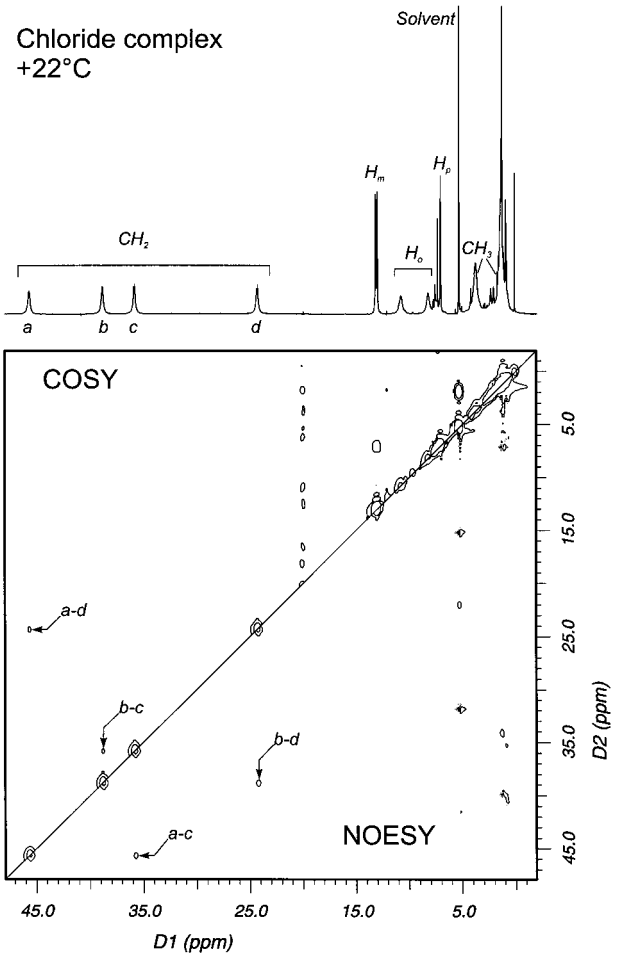

Figure 6. (Top) 1D spectrum of [(OETPP)FeCl] at 22 °C. (Above the diagonal) The magnitude-mode COSY-45 spectrum of [(OETPP)-FeCl] at 22 °C. Spectral parameters: 512 × 128 real points, 400 transients/increment, 31 ms acquisition time, 250 ms delay, 16.5 kHz spectral width (only 15.0 kHz region shown). Processed with squared sine bell apodization (10 ms for the first dimension, 4 ms for the second). (Below the diagonal) The NOESY spectrum of [(OETPP)-FeCl] at 22 °C. 256 × 80 complex points, 48 transients/increment, 10 ms mixing time, 15 ms acquisition time, 500 ms delay, 16.6 kHz spectral width (only 15.0 kHz region shown). Processed with Gaussian apodization (17 ms, 8 ms). The cross-peaks are of positive phase and therefore are due to chemical exchange. The cross-peak pattern for the methylene resonances is different from that of the COSY spectrum.

Table 2. Chemical Shifts of Proton Resonances of [(OETPP)FeCl], Recorded in CD_2Cl_2 at 22 °C

chemical shift (ppm)	assignment	chemical shift (ppm)	assignment
45.69	methylene *a*	10.77	ortho-phenyl
38.85	methylene *b*	8.21	ortho-phenyl
35.85	methylene *c*	7.06	para-phenyl
24.31	methylene *d*	3.75	methyl
13.15	meta-phenyl	1.28	methyl
13.00	meta-phenyl		

β-carbons. Other possible explanations were also considered, and found to be inapplicable to this case. The increased porphyrin-to-metal σ contribution, which causes the increased paramagnetic shift and spread of the methylene signals in low-symmetry (C_1) high-spin iron(III) chlorins,[110] is expected to

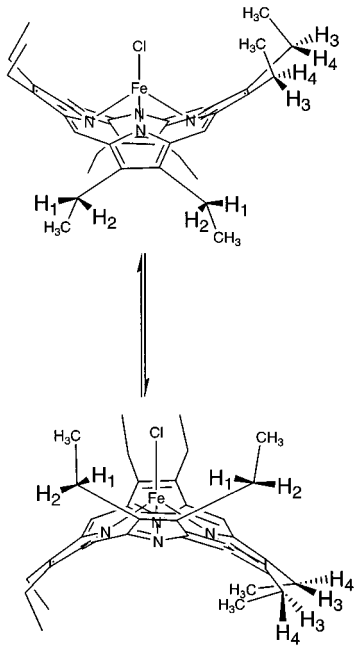

Figure 7. Schematic drawing of the chloride complex showing the four different types of methylene protons (marked H_1-H_4). (The phenyls are omitted for clarity.) The ring inversion results in exchange between methylene protons. Note that the "inner" protons become "outer" with the inversion, and vice versa.

cause an increased shift, but not spread, in the more symmetrical (C_{2v}) OETPP complexes. The mixing of the d_{z^2} and $d_{x^2-y^2}$ orbitals (both a_1 in C_{2v}) and the subsequent breaking of the axial symmetry, reported by Cheng and Chen,[111] does not influence the spin density at the pyrrole β position, because neither of these metal orbitals matches in symmetry the porphyrin a_{1u} (D_{4h}) (a_2 in C_{2v}) or e_u (D_{4h}) (b_1 and b_2 in C_{2v}), which are the only frontier orbitals with significant electron density at the pyrrole β-carbons.

The Curie plots (spectra recorded over the range 207−298 K) for the methylene protons *a* and *d* (Figure S2, Supporting Information) are significantly nonlinear. The methylene *c* resonance, although it appears to have only small curvature, extrapolates to a nondiamagnetic position at $T^{-1} = 0$. Only the plot for the methylene *b* resonance shows Curie behavior. The non-Curie behavior is probably due to a combination of (1) the restricted rotation of the ethyl groups at progressively lower temperatures[107,108,112] and (2) the contribution from the T^{-2} dipolar shift term associated with systems in which $S > {}^1/_2$.[113] The geminal pair, resonances *b*,*c* (determined by COSY, vide infra), show very similar slopes. The other geminal pair, resonances *a*,*d*, on the other hand, have completely different slopes, although they do appear to converge at temperatures higher than those of the NMR measurements.

The cross-peaks in the COSY spectrum (Figure 6, above the diagonal) arise from *J*-coupling between geminal methylene protons. In contrast, the positive-phase cross-peaks in the NOESY/EXSY spectrum (Figure 6, below the diagonal) arise from chemical exchange between the "inner-up" and "outer-down" and also the "outer-up" and "inner-down" methylene protons (Figure 7). Molecular mechanics calculations[114] indicate

(109) La Mar, G. N.; Eaton, G. R.; Holm, R. H.; Walker, F. A. *J. Am. Chem. Soc.* **1973**, *95*, 63−75.
(110) Pawlick, M. J.; Miller, P. K.; Sullivan, E. P., Jr.; Levstik, M. A.; Almond, D. A.; Strauss, S. H. *J. Am. Chem. Soc.* **1988**, *110*, 3007−3012.
(111) Cheng, R. J.; Chen, P. Y. *Chem. Eur. J.* **1999**, *5*, 1708−1715.
(112) Isaac, M. F.; Lin, Q.; Simonis, U.; Suffian, D. J.; Wilson, D. L.; Walker, F. A. *Inorg. Chem.* **1993**, *32*, 4030−4041.
(113) Kurland, R. J.; McGarvey, B. R. *J. Magn. Reson.* **1970**, *2*, 286−301.
(114) Medforth, C. J.; Shelnutt, J. A. Unpublished results.

that ethyl rotation is much faster than macrocycle inversion, and therefore the true rates of these two processes are not coincident. Nevertheless, because the equatorial species (i.e. ethyls pointing below the upward-saddled parts of the macrocycle[60]) are too short-lived to be detected by NMR, the only observed ethyl rotation process in the NOESY/EXSY spectra is that of an axial ethyl (i.e., ethyl pointing above the upward-saddled parts of the macrocycle[60]) converting to another axial ethyl of the inverted macrocycle. This is to say that the *detected* ethyl rotation correlates with macrocycle inversion. All proton resonance assignments are listed in Table 2.

The EPR spectrum (X-band, 4 K in CH_2Cl_2, Figure S3 in the Supporting Information) contains signals at $g = 6.27$, 5.26, and 1.99. The $g = 5.26$ peak is indicative of some admixture of the intermediate ($S = {}^3/_2$) spin state into the high ($S = {}^5/_2$) spin state, as shown first by Cheng et al.,[17] albeit at much smaller percentage than originally reported. The g value found in this study is more consistent with an admixture of 4−10%, as reported by Weiss et al.[49]

Proton NMR Studies of the Bis-ligand Complexes, [(OETPP)FeL$_2$]Cl. The low-spin bis-ligand complexes of (OETPP)FeCl were prepared by addition of an excess (1−2 equiv for *N*-MeIm and 4-NMe$_2$Py and 4−5 equiv for 2-MeImH) of the desired ligand to the starting material. The crystallographic data discussed above indicate that the peripheral substituents form cavities which can orient the planar axial ligands along or near the N(por)−Fe−N(por) axes. Assuming that macrocycle inversion is slow on the NMR time scale, the number of methylene resonances can be used to determine the effective symmetry of the bis-ligand complexes in solution. The number of methylene resonances observed increases as the symmetry is lowered: two (D_{2d}), four (C_{2v}), and eight (C_2). The idealized symmetries from the crystallographic data for the five- and six-coordinate (OETPP)Fe^{III} complexes, presented above, are C_{2v} and D_{2d}, respectively. Depending on the symmetry of the axial ligands, the low-spin Fe(III) porphyrinate symmetry can be lowered to C_2. Similar symmetry arguments were invoked for the highly ruffled, six-coordinate low-spin Fe(III) chiroporphyrins.[59] The resonance assignments were made on the basis of relative areas, 2D NMR data, temperature dependence, and relaxation times.

At least two general types of dynamic processes are expected and observed in six-coordinate [(OETPP)FeL$_2$]$^+$ complexes: (1) ligand exchange, in which a coordinated ligand dissociates and is rapidly replaced by a formerly free ligand molecule[106−108,115]

$$[(\mathrm{OETPP})\mathrm{FeL_2}]^+ \rightleftarrows [(\mathrm{OETPP})\mathrm{FeL}]^+ + \mathrm{L} \quad \downarrow \mathrm{L}^* \quad [(\mathrm{OETPP})\mathrm{Fe(L)(L^*)}]^+ \qquad (1)$$

and (2) macrocycle inversion, where the saddled porphyrinate ring inverts, such that the two pyrrole rings that were originally displaced above the mean plane of the macrocycle become displaced below, and those that were originally displaced below become displaced above the mean plane of the macrocycle.[12,116] Macrocycle inversion has been suggested to occur via a ruffled transition state,[114] and it has been possible in this work to observe, by X-ray crystallography, a partially saddled, partially ruffled conformation of [(OETPP)Fe(4-NMe$_2$Py)$_2$]$^+$ that may be on the reaction coordinate for ring inversion (vide supra).

Two additional chemical exchange processes are known or expected to occur in these highly saddled porphyrinate complexes: (3) axial ligand rotation, which, as we will show, occurs in concert with macrocycle inversion, and (4) substituent (ethyl, as in the present case, and phenyl)[117,118] rotation. Substituent rotational barriers in sterically crowded porphyrins can be significantly lower than expected if the type of distortion facilitates rotation by moving the substituent out-of-plane.[118] Previous crystallographic studies on dodecaphenylporphyrins[118] (DPPs) have suggested that they are more conformationally flexible than other sterically crowded porphyrins, and therefore are more susceptible to macrocycle inversion. Molecular mechanics calculations suggest that the saddle inversion occurs through a ruffled intermediate.[114] Also, molecular mechanics calculations[114] have previously suggested that in the saddled OETPPH$_2$ and its metal complexes, as well as in OEPH$_2$ and its metal complexes,[119] ethyl rotation has a low energy barrier. Thus, for OETPPH$_2$ and its metal complexes, ethyl substituents may interchange from axial to equatorial and back to axial again a number of times[60] before inversion of a saddled porphyrin. While this is quite likely the case, it could not be proven by the NMR techniques utilized in this study; it is found in the present work that the ethyl groups spend at least the majority of their time in axial positions so that separate resonances are observed for "inner" and "outer" methylene protons, but not for axial and equatorial ethyl groups. Upon macrocycle inversion, the "inner" protons become "outer" and vice versa, suggesting rapid ethyl rotation but slower macrocycle inversion.

Proton NMR Studies of the Bis-(*N*-methylimidazole) Complex, [(OETPP)Fe(*N*-MeIm)$_2$]Cl. The 1D ^{1}H spectra of the bis-(*N*-MeIm) complex at −30 and −80 °C are shown in Figure 8. In addition to ethyl and phenyl resonances, free and ligated imidazole proton resonances are seen. The two methylene peaks, identified using 2D NMR experiments (vide infra), are found in the shift range of 6−14 ppm and indicate effective D_{2d} symmetry, despite the unsymmetrical nature of the *N*-MeIm ligand. It thus appears that, as observed previously for other bis-(*N*-MeIm) complexes,[112,120] the *N*-methyl group is far enough from the binding site that it does not influence the NMR-detected symmetry. The large separation between the methylene resonances, and their similar average chemical shift to that of [OEPFe(NMeIm)$_2$]$^+$,[108,112] are consistent with the $(d_{xy})^2(d_{xz},d_{yz})^3$ ground state of iron(III),[108,112] for which the spin density is concentrated at the pyrrole β positions. They are inconsistent with the $(d_{xz},d_{yz})^4(d_{xy})^1$ state, for which the methylene peaks are found narrowly spaced in the diamagnetic region because of the concentration of the spin density at the *meso* positions.[37] Thus, we find that the saddled macrocycle conformation tends to favor the $(d_{xy})^2(d_{xz},d_{yz})^3$ state for low-spin ferrihemes, rather than the $(d_{xz},d_{yz})^4(d_{xy})^1$ state, which has often been observed in highly ruffled porphyrins.[19,24,37,59] This conclusion is thus totally consistent with that based on the EPR data shown in Figure 5.

The resonances belonging to the protons of [(OETPP)Fe(*N*-MeIm)$_2$]$^+$ shift significantly with temperature. Peak *k* (which is obscured by a strong impurity signal at 2.25 ppm at −30 °C,

(115) La Mar, G. N.; Walker, F. A. *J. Am. Chem. Soc.* **1972**, *94*, 8607−8608.

(116) Medforth, C. J. In *The Porphyrin Handbook*; Kadish, K. M., Smith, K. M., Guilard, R., Eds.; Academic Press: San Diego, 2000; Vol. 5, Chapter 35, pp 70−73 and references therein.

(117) Senge, M. O.; Medforth, C. J.; Forsyth, T. P.; Lee, D. A.; Olmstead, M. M.; Jentzen, W.; Pandey, R. K.; Shelnutt, J. A.; Smith, K. M. *Inorg. Chem.* **1997**, *36*, 1149−1163.

(118) Muzzi, C. M.; Medforth, C. J.; Voss, L.; Cancilla, M.; Lebrilla, C.; Ma, J.-G.; Shelnutt, J. A.; Smith, K. M. *Tetrahedron Lett.* **1999**, *40*, 6159−6162.

(119) Medforth, C. J. In *The Porphyrin Handbook*; Kadish, K. M., Smith, K. M., Guilard, R., Eds.; Academic Press: San Diego, CA, 2000; Vol. 5, Chapter 35, pp 67−68.

(120) Shokhirev, N. V.; Walker, F. A. *J. Phys. Chem.* **1995**, *99*, 17795−17084.

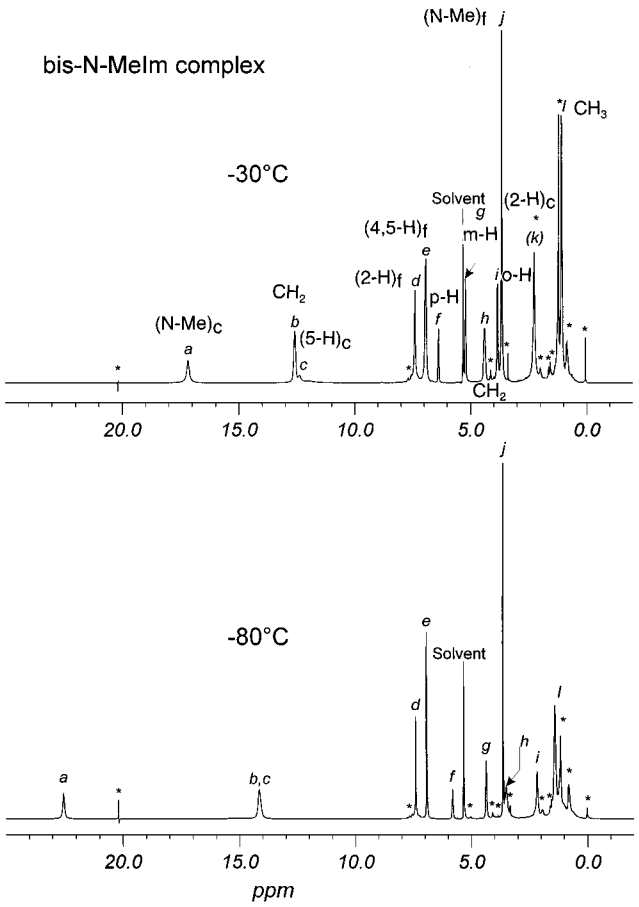

Figure 8. 1D ^{1}H NMR spectra of [(OETPP)Fe(*N*-MeIm)$_2$]Cl at −30 and −80 °C. The resonances of the porphyrin and complexed (c) and free (f) ligand are labeled *a*−*l* and the assignments given; resonances of the solvent ($CHDCl_2$) and impurity peaks are marked (*). Note the change in chemical shift with change in temperature of all the peaks except for those of the solvent, impurities, and the free ligand.

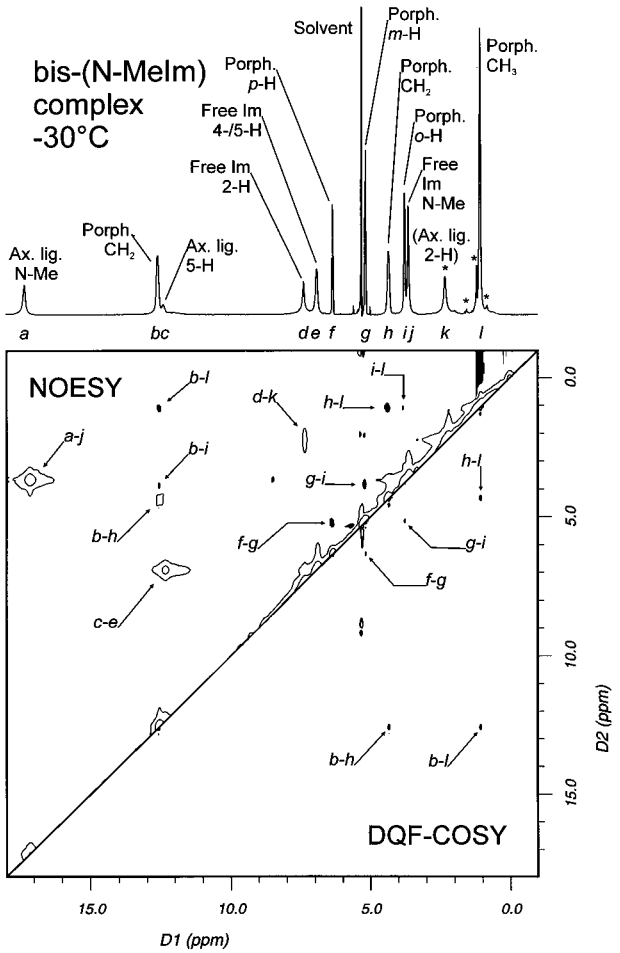

Figure 9. (Above the diagonal) NOESY/EXSY spectrum of [(OETPP)-Fe(*N*-MeIm)$_2$]Cl at −30 °C in CD_2Cl_2. Acquisition parameters: 512 × 64 complex points, 80 transients/increment, 50 ms mixing time, 85 ms acquisition time, 335 ms delay, 6.0 kHz spectral width (only 5.7 kHz region shown). Processed with Gaussian apodization (25 ms for the first dimension, 13 ms for the second). The negative-phase cross-peaks are shown as solid spots. (Below the diagonal) The DQF-COSY spectrum of [(OETPP)Fe(*N*-MeIm)$_2$]Cl at −30 °C. Acquisition parameters: 512 × 64 complex points, 6.6 kHz spectral width (only 5.7 kHz region shown), 78 ms acquisition time, 4000 ms delay time between transients, 16 transients per increment. Gauss−Lorenzian transformation was applied before each Fourier transformation. (First dimension: 100 ms line narrowing, 33 ms Gaussian. Second dimension: 30 ms line narrowing, 10 ms Gaussian.) The small unlabeled spots in the NOESY spectrum are believed to be due to noise or other artifacts, because they are not present on the other side of the diagonal (not shown).

but is detected by a strong chemical exchange cross-peak with the 2-H resonance of free *N*-MeIm in the NOESY/EXSY spectrum of Figure 9, above the diagonal), is seen as a shoulder at 2.1 ppm at −40 °C. At this temperature, the (now weak) chemical exchange cross-peak clearly shows that this shoulder is the bound 2-H resonance (Figure S4, Supporting Information). This 2-H resonance shifts to higher shielding as the temperature is lowered, but cannot be detected at −60 °C due to overlap with other peaks, and probable extreme broadening. Both the 2-H and 4-H resonances of the coordinated *N*-MeIm ligands are typically very broad.[108,112] The T_1 relaxation times (−30 and −80 °C, Table 4) may be categorized into two groups: short (about 50 ms, porphyrin methylene and coordinated ligand protons) and long (about 300 ms, porphyrin phenyl and methyl, and free imidazole protons). The average T_1 of the "short" group was used as the mixing time for the NOESY/EXSY experiments (vide infra).

The negative-phase (i.e., opposite that of the diagonal peaks) cross-peaks in the NOESY/EXSY spectra taken at −30 °C (Figure 9, above the diagonal) indicate that at this temperature the complex is in the small-molecule (positive NOE) regime. The chemical exchange cross-peaks *a*-*j*, *c*-*e*, and *d*-*k*, together with the previously assigned free *N*-MeIm peaks (*d*, *e*, *j*) from the 1D spectrum in CD_2Cl_2 (not shown), allow the assignment of *a*, *c*, and *k* to the coordinated axial ligand *N*-methyl, 5-H, and 2-H protons. As discussed above, the signal from the axial ligand 2-H is at 2.25 ppm at −30 °C (buried under the more intense impurity resonance at that chemical shift) and shifts to higher shielding as the temperature is decreased. The 4-H peak was not positively identified, although an extremely broad signal (>1000 Hz line width) whose shift is temperature-dependent (12.0 ppm at −30 °C, 15.0 ppm at −80 °C, not marked) might be that of the ligand 4-H. All resonances at −30 and −80 °C are listed, together with their T_1 values and assignments, in Table 3.

The NOE cross-peaks *h*-*l* in the NOESY/EXSY spectrum are also found in the COSY spectrum (−30 °C, Figure 9, below the diagonal). The peak *l* is assigned to the porphyrin methyl protons because of its position, T_1, and behavior (1.2 ppm, small temperature dependence of its chemical shift). Therefore, resonance *h* is assigned to one of the porphyrin methylene protons. On the basis of the COSY spectrum, resonance *b* is assigned to its geminal partner. The positive-phase cross-peaks between the two methylene protons (*b*−*h*) in the NOESY/EXSY

Table 3. Chemical Shifts and T_1 Relaxation Times for [(OETPP)Fe(*N*-MeIm)$_2$]Cl in CD_2Cl_2 at Two Temperatures

	−30 °C		−80 °C		
peak	shift (ppm)	T_1 (s)	shift (ppm)	T_1 (s)	assignment
a	17.18	0.178(8)	22.53	0.0235(3)	axial ligand *N*-Me
b	12.58	0.0619(4)	14.15	0.0386(3)	porphyrin methylene, outer
c	12.38	0.099(8)	14.15	hidden behind *b*	axial ligand 5-H
	∼12.0	very broad	∼15.0	very broad	axial ligand 4-H?
d	7.39	0.045(2)	7.39	0.436(1)	free imidazole 2-H
e	6.92	0.055(2)	6.92	0.686(3)	free imidazole 4,5-H
f	6.38	0.492(3)	5.80	0.367(3)	porphyrin para-phenyl
g	5.21	0.351(2)	4.35	0.226(1)	porphyrin meta-phenyl
h	4.39	0.0667(2)	3.49	0.046(1)	porphyrin methylene, inner
i	3.83	0.0768(3)	2.16	0.041(1)	porphyrin ortho-phenyl
j	3.65	0.195(2)	3.62	0.804(8)	free imidazole *N*-Me
k	2.25		not observed		axial ligand 2-H
l	1.21	0.057(2)	1.15	0.0277(6)	porphyrin methyl

Table 4. Chemical Shifts and T_1 Relaxation Times for [(OETPP)Fe(4-NMe$_2$Py)$_2$]Cl in CD_2Cl_2 at Two Temperatures

	−20 °C		−70 °C		
peak	shift (ppm)	T_1 (s)	shift (ppm)	T_1 (s)	assignment
a	15.17	0.170(5)	19.71	0.0671(4)	bound ligand N−CH_3
b	14.27	0.041(2)	17.04	0.0201(1)	bound ligand 3,5-H
c	12.24	0.0698(5)	12.80	0.0619(2)	porphyrin methylene, outer
d	8.15	0.0088(2)	8.07	0.0766(2)	free ligand 2,6-H
e	6.52	0.0470(2)	6.47	0.2074(5)	free ligand 3,5-H
f	6.34	0.32(3)	5.69	0.449(5)	porphyrin para-phenyl
g	5.36	0.46(2)	4.53	0.309(1)	porphyrin meta-phenyl
h	4.14	overlapped with impurity peak	2.96	0.11(2)	porphyrin methylene, inner
k	3.95	0.093(3)	2.11	0.076(4)	porphyrin ortho-phenyl
l	2.98	0.1874(3)	2.96	0.336(3)	free ligand N−CH_3
m	1.07	0.100(9)	1.47	0.046(2)	porphyrin methyl
n	−1.89	very short	−2.79	0.0025(7)	bound ligand 2,6-H

spectrum indicate that these methylene protons are in chemical exchange. (In the NOESY/EXSY spectrum taken at −40 °C (not shown), the cross-peaks from the *b*-*h* set are of *negative* phase, indicating that at this temperature only NOEs are detected, and the chemical exchange has become immeasurably slow on the NMR time scale.)

The sign of the NOE crosses from positive to negative at approximately −60 °C. The NOESY/EXSY spectrum taken at this temperature contains no interpretable NOE cross-peaks above the noise level, and is not shown herein. At −80 °C, the NOE is negative, and therefore the dipolar cross-peaks have the same phase (positive) as the diagonal and chemical exchange peaks,[121] as observed in the NOESY/EXSY spectrum at this temperature (not shown).

(121) Cavanagh, J.; Fairbrother, W. J.; Palmer, A. G., III; Skelton, N. J. *Proton NMR Spectroscopy: Principles and Practice*; Academic Press: San Diego, 1996; pp 394−402.

The cross-peak pattern between *f*, *g*, and *i*, seen in both NOESY and COSY spectra, indicates that these three signals originate from the phenyl protons, in which the ortho−meta and meta−para pairs, but not the ortho−para pair, are expected to give rise to both scalar and NOE cross-peaks. Since peak *i* is approximately twice as large as peak *f*, the former is assigned to the ortho and the latter to the para protons. The dipolar-coupling cross-peak *b*−*i* results from the proximity of one type of methylene protons to the ortho-phenyl protons. This through-space interaction indicates that *b* arises from the "outer" methylene protons, and consequently, *h* arises from the "inner" methylene protons (assignments and chemical shifts at two temperatures listed in Table 3).

The number of methylene resonances of [OETPPFe(*N*-MeIm)$_2$]$^+$Cl$^-$ is consistent with the idealized D_{2d} symmetry of the complex, in which the average orientation of the axial ligands is mutually perpendicular and positioned over the nitrogens. This idealized D_{2d} symmetry, however, still permits the axial ligands to take a wide range of rotational positions in solution; only the *average* chemical shift (which represents the average position) over the time scale of the NMR measurements can be observed. It is clear that at −30 °C ligand rotation and the associated porphyrin ring inversion are slow on the NMR time scale, and thus the "inner" and "outer" methylene-H resonances are separate, yet have strong chemical exchange (EXSY) cross-peaks (Figure 9, above the diagonal); although *N*-MeIm is the least hindered ligand investigated herein, we do not believe that it can rotate freely without porphyrin ring inversion.

The NMR data obtained herein do not preclude a lower symmetry being observed in the crystalline state. Also, the number of methylene signals is consistent with the detection of only the axial conformation of the ethyl groups, even though they are believed to rotate rapidly,[114] and therefore the correlation of the *observed* ethyl rotation with macrocycle inversion (vide supra).

The Curie plot for [(OETPP)Fe(*N*-MeIm)$_2$]Cl (Figure S5, Supporting Information) shows significant curvature for most resonances, with nondiamagnetic shift intercepts. Previous studies of ferrihemes with axial imidazole ligands show non-diamagnetic shift intercepts and/or curved temperature dependences of the Curie plots due to the following factors: (1) hindered rotation of ethyl groups at lower temperatures;[112] (2) axial ligand alignment that deviates from perpendicularity due to the Jahn−Teller distortion;[20,94] and (3) thermal excitation from the $(d_{xy})^2(d_{xz},d_{yz})^3$ to the $(d_{xz},d_{yz})^4(d_{xy})^1$ state.[59,121] Because these factors cannot be deconvoluted in this case, the Curie plot cannot be used here as a reliable indicator for the orientation of the ligands, or of possible thermal excitation from the ground state to an excited state.

Proton NMR Studies of the Bis-(4-(dimethylamino)-pyridine) Complex, [(OETPP)Fe(4-NMe$_2$Py)$_2$]Cl. The 1D NMR spectra of the bis-(4-NMe$_2$Py) complex were well resolved below −20 °C (Figure 10). The two methylene peaks, identified using the COSY spectrum (vide infra), are found in the 4.1−12.2 ppm region at −20 °C (assignments and chemical shifts given in Table 4). As for the bis-(*N*-MeIm) complex, their positions are consistent with the $(d_{xy})^2(d_{xz},d_{yz})^3$ ground state of low-spin Fe(III). The number of methylene proton signals (two) is again consistent with D_{2d} symmetry in solution. The protons not corresponding to the free pyridine or to impurities show non-Curie temperature dependence for their chemical shifts (Figure S6, Supporting Information). The non-Curie behavior has many potential contributions that cannot be deconvoluted, as already discussed above for the bis-(*N*-MeIm) complex. Peak

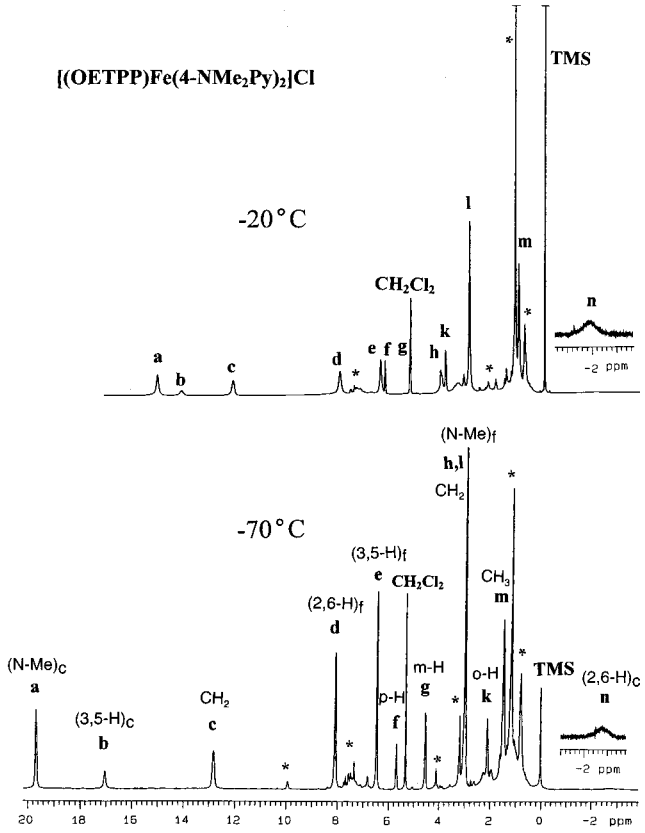

Figure 10. 1D ^{1}H NMR spectra of [(OETPP)Fe(4-NMe$_2$Py)$_2$]Cl at −20 and −70 °C in CD_2Cl_2. The solvent and TMS resonances, and those of impurities (*), are marked. Resonances of the porphyrin and complexed (c) and free (f) ligand are marked and labeled a−n.

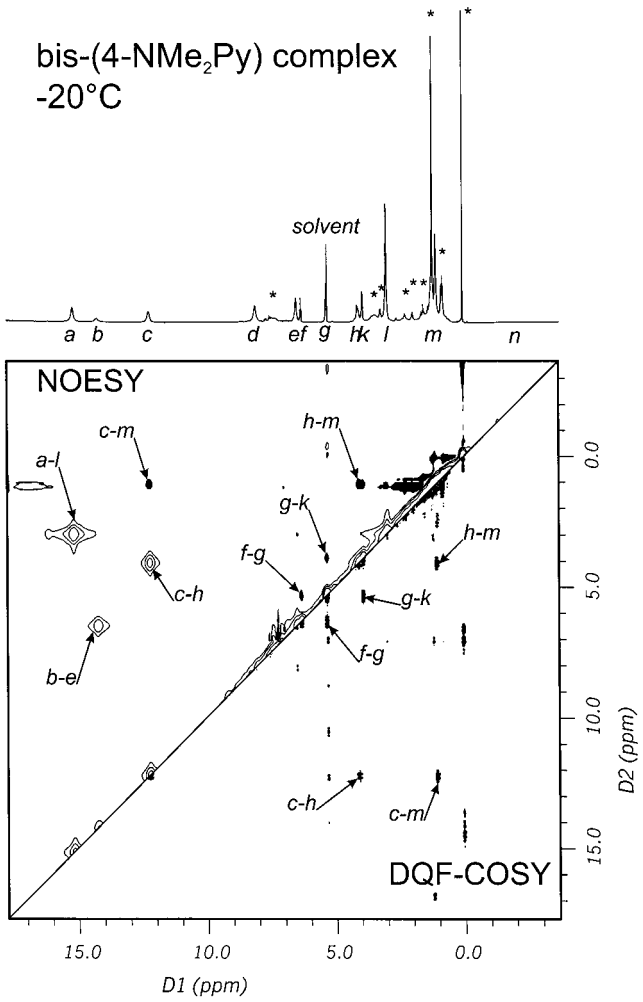

Figure 11. (Above the diagonal) NOESY spectrum of [(OETPP)Fe(4-NMe$_2$Py)$_2$]Cl in CD_2Cl_2 at −20 °C. The spectrum was acquired with a spectral bandwidth of 6.44 kHz, with 512 × 128 complex points, 32 transients per t_1 increment, a 79 ms mixing time, and 320 ms relaxation delay between increments. The spectrum was processed after application of Gaussian window functions (17 ms, 8 ms). (Below the diagonal) DQF-COSY spectrum of [(OETPP)Fe(4-NMe$_2$Py)$_2$]Cl at −20 °C. The spectrum was acquired with a spectral bandwidth of 6.44 kHz, with 512 × 128 complex points, 32 transients per increment, 79 ms acquisition time, and 380 ms relaxation delay between transients. The spectrum was processed after application of sine bell window functions (39 ms for the first dimension and 10 ms for the second). See Figure 10 and Table 4 for complete assignments.

n corresponding to the axial ligand 2,6-H (assigned by analogy to those of the corresponding (TMP)Fe^{III} bis-(pyridine) complexes[24,107]) is very broad, which is consistent with dipolar relaxation that has a $1/r^6$ dependence on the proximity of these protons to the iron.[122] As in the bis-(*N*-MeIm) complex, the T_1 relaxation times for the bis-(4-NMe$_2$Py) complex (Table 4) can be divided into two groups: short (about 50 ms for methylene, phenyl ortho-, and free pyridine 2,6- and 3,5-protons) and long (200−450 ms for methyl, phenyl meta- and para-, and free pyridine *N*-Me protons). The T_1 values of the free pyridine protons (Table 4) substantially increase as the temperature is lowered; those of the ligated molecules, on the other hand, decrease with decreasing temperature.

The NOESY/EXSY spectrum taken at −20 °C (Figure 11, above the diagonal) shows three pairs of significant chemical exchange cross-peaks. Two of them, *a*-*l* and *b*-*e*, are from the chemical exchange between the free and ligated 4-NMe$_2$Py molecules. The third (*c*-*h*) is from chemical exchange between the methylene protons resulting from macrocycle ring inversion/ligand rotation/ethyl rotation. Also, the spectrum shows NOE cross-peaks which are caused by the interactions among the phenyl protons, *f*-*g* (para−meta) and *g*-*k* (meta−ortho). The phenyl protons were also identified by the cross-peaks that appear in the corresponding positions in the DQF-COSY spectrum (Figure 11 below the diagonal) and the *J*-coupling patterns observed in the 1D spectra. The other NOE peaks are *h*-*m* (inner methylene−methyl), *c*-*k* (outer methylene−phenyl ortho), and *c*-*m* (outer methylene−methyl). Because of the *c*-*k* cross-peak, it is possible to assign the "outer" and "inner" methylene protons. The ROESY spectra of the bis-(4-NMe$_2$-Py) complex at −60 °C (Figure S7, Supporting Information), unlike those of the bis-(*N*-MeIm) complex, were contaminated with TOCSY cross-peaks. This spectrum contained a pair of NOE cross-peaks from the interaction between the methyl protons of the ethyl groups and the phenyl ortho protons (*k*-*m*). According to the NOESY and ROESY data, the axial ligand exchange becomes too slow on the NMR time scale to be observed below −60 °C, and macrocycle inversion is no longer observed below about −50 °C. The NOE crossover point is also at about −50 °C.

Proton NMR Studies of the Bis-(2-methylimidazole) Complex, [(OETPP)Fe(2-MeImH)$_2$]Cl. Because of ligand exchange and macrocycle inversion, both of which were evident to extremely low temperatures, interpretable NMR spectra of the bis-(2-MeImH) complex could be obtained only below −70 °C, even when an excess of ligand (1:6 (OETPP)Fe^{III}/2-MeImH) was used. The 1D NMR spectrum (Figure 12, top) exhibits more

(122) Unger, S. W.; Jue, T.; La Mar, G. N. *J. Magn. Reson.* **1985**, *61*, 448−456.

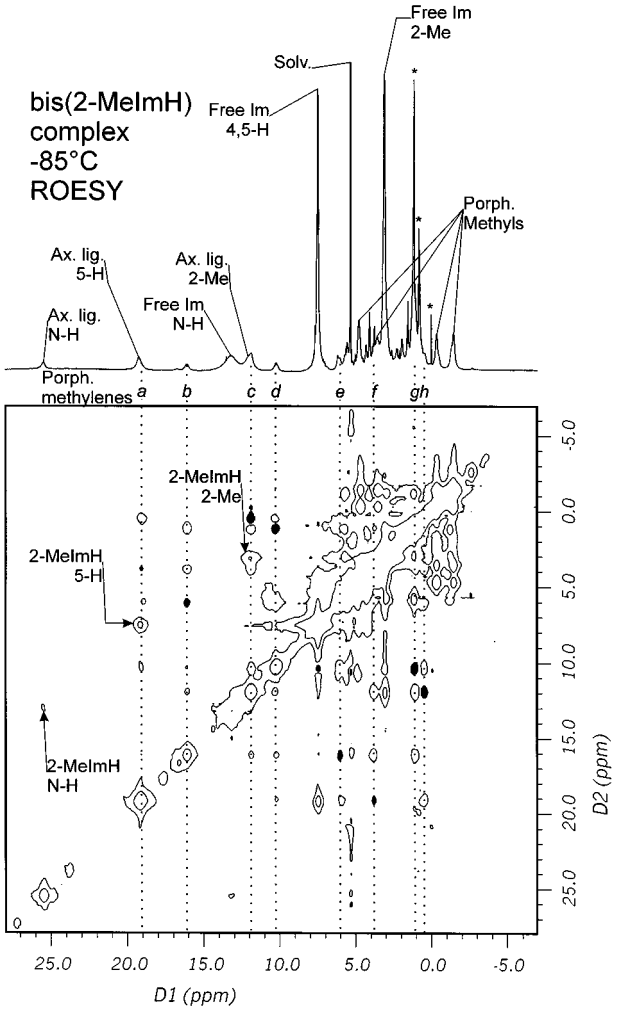

Figure 12. (Top) 1D NMR spectrum of $[(OETPP)Fe(2\text{-}MeImH)_2]Cl$ at −85 °C in CD_2Cl_2. (Bottom) ROESY spectrum of $[(OETPP)Fe(2\text{-}MeImH)_2]Cl$ at −85 °C. 512 × 160 complex points, 96 transients per increment, 10 ms mixing time, 49 ms acquisition time, 150 ms delay, 10.5 kHz spectral width, 10.5 kHz spin lock field. Processed with Gaussian apodization (17 ms for the first dimension, 8 ms for the second).

proton resonances (eight methylene resonances, for example) than those of the bis-(*N*-MeIm) and bis-(4-NMe_2Py) complexes (Figures 8 and 10), because of the proximity of the axial ligand 2-Me to the porphyrin ring, which lowers the symmetry to C_2. The T_1 values, which are short even at −90 °C, indicate that chemical exchange (both ligand exchange and macrocycle inversion) is significant even near the freezing point of the solvent.

The ROESY spectrum at −85 °C (Figure 12), taken using a short mixing time (10 ms), is relatively easy to interpret because of the following: (1) the two types of cross-peaks (NOE and chemical exchange) have different phase[121] and (2) only a few chemical exchange cross-peaks are present, because only the faster of the slow chemical exchange processes are detected at the short mixing time. For the ROESY spectrum, the transverse field B_1 was set at about 10 kHz, a typical value for the spectral bandwidth of low-spin ferrihemes at 300 MHz. Although the existing literature warns that TOCSY peaks could contaminate the ROESY spectrum if the B_1 field is set too high,[121] we found no significant problem in some previous studies[123] or the present

(123) Shokhireva, T. Kh.; Nesset, M. J. M.; Walker, F. A. *Inorg. Chim. Acta* **1998**, *272*, 204−210.

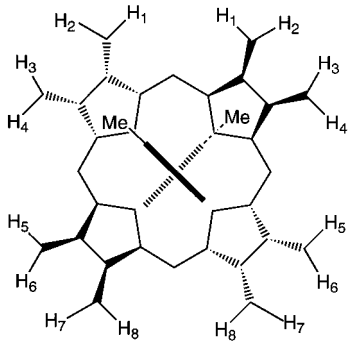

Figure 13. Schematic drawing of $[(OETPP)Fe(2\text{-}MeImH)_2]^+$, depicting the methylene protons. Depending on their distance to one of the 2-Me groups of the axial ligands, the methylene protons can be classified into eight different types.

Table 5. Chemical Shifts of Proton Resonances of $[(OETPP)Fe(2\text{-}MeImH)_2]Cl$ in CD_2Cl_2 at −85 °C

shift (ppm)	assignment	shift (ppm)	assignment
25.49	axial ligand NH	6.02	porphyrin methylene *e*
19.21	axial ligand 5-H	5.68	porphyrin phenyl
19.10	porphyrin methylene *a*	4.68	porphyrin methyl
16.67	porphyrin phenyl	3.76	porphyrin methylene *f*
16.11	porphyrin methylene *b*	3.53	porphyrin methyl
not observed	axial ligand 4-H	2.91	free imidazole 2-CH_3
13.34	free imidazole NH	1.10	porphyrin phenyl
11.98	axial ligand 2-CH_3	1.00	porphyrin methylene *g*
11.87	porphyrin methylene *c*	0.42	porphyrin methylene *h*
10.24	porphyrin methylene *d*	−0.38	porphyrin methyl
7.48	free imidazole 4-H,5-H	−1.31	porphyrin phenyl
6.84	porphyrin phenyl	−1.49	porphyrin methyl

studies of the bis-(2-MeImH) complex, whereas TOCSY cross-peaks were clearly present in the ROESY spectra of the bis-(4-NMe_2Py) complex (vide supra). From the ROESY spectrum, we may identify the peaks corresponding to eight types of methylene protons (consistent with the C_2 molecular symmetry, see Figure 13), and find that the geminal partners are *a*-*f*, *b*-*e*, *c*-*h*, and *d*-*g*. The dipolar coupling pattern of the methylene protons, as well as the Curie plot (−73 to −90 °C) for the methylene proton resonances (Figure S8, Supporting Information), are consistent with assignment of the peaks *a*, *b*, *c*, and *d* to the "outer" and *e*, *f*, *g*, and *h* to the "inner" protons. Unfortunately, no methylene−phenyl NOE cross-peaks were observed for this complex, and thus further assignment of the methylene resonances is precluded. The 2-methyl, N−H, and 5-H resonances of the 2-methylimidazole ligands were identified by chemical exchange with free 2-MeImH (listed in Table 5). The 4-H resonance could not be located. As for the other two bis-(nitrogen-donor ligand) complexes of this study, the chemical shifts of the methylene and axial ligand resonances are consistent with the $(d_{xy})^2(d_{xz},d_{yz})^3$ ground state, unlike the results from highly ruffled low-spin ferrihemes with hindered axial imidazoles, whose electronic states have been shown to be a mixture of the $(d_{xy})^2(d_{xz},d_{yz})^3$ and $(d_{xz},d_{yz})^4(d_{xy})^1$ configurations.[59]

The dominance of the ROESY spectrum of $[(OETPP)Fe(2\text{-}MeImH)_2]^+$ (Figure 12) by chemical exchange cross-peaks at −85 °C is in sharp contrast to the fact that the NOESY/EXSY spectra of $[(OETPP)Fe(N\text{-}MeIm)_2]^+$ and $[(OETPP)Fe(4\text{-}NMe_2\text{-}Py)_2]^+$ lose essentially all chemical exchange cross-peaks between −40 and −60 °C. This indicates that the barrier to inversion/ligand rotation decreases in the ligand order *N*-MeIm > 4-NMe_2Py > 2-MeImH. This order probably reflects to a greater extent the destabilization of the ground state as the bulkiness of the axial ligand increases, rather than a stabilization

of the transition state in that order.[25,124] A similar situation was found in molecular mechanics calculations for [(TMP)Fe(4-CNPy)$_2$]$^+$ as compared to [(TPP)Fe(4-CNPy)$_2$]$^+$.[25]

The chemical exchange cross-peaks in the ROESY spectrum at −85 °C (Figure 12) suggest that an "outer" proton is converted predominantly[125] to an "inner" proton instead of another type of "outer" proton. Therefore, the dominant dynamic process involves macrocycle inversion with concurrent ethyl rotation. The number of methylene peaks indicates that the equatorial species are short-lived, and therefore the observed ethyl rotation is correlated with the inversion, as observed for the other two bis-ligand complexes (vide supra). In addition, each "outer" proton exchanges with only two of the possible four "inner" protons, which suggests that the inversion and the axial ligand rotation are at least partially correlated, and therefore in the dominant dynamic process the random dissociation/reassociation of both axial ligands is precluded.[125] One possible mechanism involves the inversion of the saddled macrocycle, accompanied by the simultaneous rotation of both axial ligands in the *same direction* (synchronous), which was shown to be the lowest-energy path for highly ruffled porphyrins,[62] and is undoubtedly so also for highly saddled porphyrins. On the basis of Figure 13, the simultaneous inversion/rotation would convert protons 1 to 3 or 6, 2 to 5 or 4, 3 to 8 or 1, 4 to 7 or 2, 5 to 2 or 7, 6 to 1 or 8, 7 to 4 or 5, and 8 to 6 or 3. The inability to observe NOE cross-peaks between methylene and phenyl protons precludes more detailed assignment of methylene resonances *a*−*h* to proton types 1−8. The assignments that were possible are listed in Table 5.

Conclusions

The molecular structure of [(OETPP)Fe(2-MeImH)$_2$]$^+$ shows that the axial ligands are in perpendicular planes, and that the ligand planes are rotated by 14° to the porphyrin N−Fe−N axes, while the structure of [(OETPP)Fe(4-NMe$_2$Py)$_2$]$^+$ shows that the axial ligands are not in perpendicular planes, but rather have a much smaller dihedral angle of 70°. Such flexibility in the dihedral angle between axial ligand planes for the bis-(4-NMe$_2$-Py) complex may help to explain the existence of both "large g_{max}" and normal rhombic EPR signals for the presumably less-hindered (more flexible) [(OETPP)Fe(*N*-MeIm)$_2$]$^+$ complex in frozen solution (since five-membered imidazole rings are expected to have greater rotational freedom in these saddled porphyrin complexes than six-membered pyridine rings), and demonstrates the power of the Jahn−Teller effect in determining axial ligand dihedral angles in the latter low-spin iron(III) porphyrinate. The variable-temperature 1- and 2D NMR data for the (OETPP)Fe^{III} complexes give insights into the stereochemistry and the fluxional properties of these complex ions. The 2D spectra of the five-coordinate (OETPP)FeCl show cross-peaks consistent with the expected fluxional motion in solution. Complete peak assignments of the six-coordinate [(OETPP)-Fe(*N*-MeIm)$_2$]$^+$ and [(OETPP)Fe(4-NMe$_2$Py)$_2$]$^+$ complexes were possible by a combination of NOESY/EXSY and COSY experiments. The bis-(*N*-MeIm) and bis-(4-NMe$_2$Py) complexes are fluxional at −40 °C and above, but their fluxionality becomes undetectable on the NMR time scale at −80 °C. The 2D NMR data indicate that the relative axial ligand orientation is, on average, perpendicular in these dynamic complexes. The Curie plots are affected by many factors, and the contributions from these cannot be deconvoluted. The six-coordinate [(OETPP)Fe(2-MeImH)$_2$]$^+$ shows a much more complicated peak pattern than either of the other two six-coordinate complexes, due to the lower symmetry created by the unsymmetrical 2-MeImH ligands. A partial assignment of the methylene peaks is possible by use of ROESY spectra. The NMR spectrum of the complex is resolved only at very low temperatures (−70 to −90 °C), and the complex is fluxional over this temperature range.

Acknowledgment. The financial support of the National Institutes of Health, Grants DK 31038 (F.A.W.) and HL 22252 (K.M.S.), and the Division of Chemical Sciences, U.S. Department of Energy, Contract DE-AC02-98CH10886 (K.M.B., M.W.R., D.M.), is gratefully acknowledged. C.J.M. acknowledges financial support from Professor John Shelnutt (Sandia National Laboratories and University of New Mexico). F.A.W. thanks Dr. So Iwata for providing the 2.5 Å resolution coordinates for the cytochrome bc_1 complex and Dr. Sue Roberts for measuring the angles of the axial ligand planes of the *b* hemes.

Supporting Information Available: Crystal structure parameters, atomic coordinates, NMR Curie plots, 2D NMR spectra at additional temperatures, and the EPR spectrum of [(OETPP)FeCl] (PDF). This material is available free of charge via the Internet at http://pubs.acs.org.

JA004053S

(124) Barkigia, K. M.; Nurco, D. J.; Renner, M. W.; Melamed, D.; Smith, K. M.; Fajer, J. *J. Phys. Chem. B* **1998**, *102*, 322−326.

(125) The ROESY spectrum does contain very small "outer" −"outer" chemical exchange peaks and also the axial ligand-free imidazole exchange peaks (except for 1-H). This indicates that some dissociation/reassociation *does* occur. However, this occurs independently and apart from the macrocycle inversion.